JOURNAL OF GEOPHYSICAL RESEARCH, VOL. 114, D15303, doi:10.1029/2009JD011724, 2009

A global sensitivity analysis and Bayesian inference framework for improving the parameter estimation and prediction of a process-based Terrestrial Ecosystem Model

Jinyun Tang[1,2] and Qianlai Zhuang[1,2,3]

Received 7 January 2009; revised 5 March 2009; accepted 9 June 2009; published 11 August 2009.

[1] A global sensitivity analysis and Bayesian inference framework was developed for improving the parameterization and predictability of a monthly time step process-based biogeochemistry model. Using a Latin Hypercube sampler and an existing Terrestrial Ecosystem Model (TEM), a set of 500,000 Monte Carlo ensemble simulations was conducted for a black spruce forest ecosystem. A global sensitivity analysis was then conducted to identify the key model parameters and examine the interaction structures among TEM parameters. Bayesian inference analysis was also performed using these ensemble simulations and eddy flux data of carbon, latent heat flux, and MODIS gross primary production (GPP) to reduce the uncertainty of parameter estimation and prediction of TEM. We found that (1) the simulated carbon fluxes are mostly affected by parameters of the maximum rate of photosynthesis (CMAX), the half-saturation constant for CO_2 uptake by plants (k_c), the half-saturation constant for Photosynthetically Active Radiation used by plants (k_i), and the change in autotrophic respiration due to 10°C temperature increase (RHQ10); (2) the effect of parameters on seasonal carbon dynamics varies from one parameter to another during a year; (3) to well constrain the uncertainties of TEM predictions and parameters using the Bayesian inference technique, at least two different fluxes of NEP, GPP, and ecosystem respiration (RESP) are required; and (4) different assumptions of the error structures of the flux data used in the Bayesian inference analysis result in different uncertainty bounds of the posterior parameters and model predictions. We further found that, using the Bayesian framework and eddy flux and satellite data, the uncertainty of simulated carbon fluxes has been remarkably reduced. The developed global sensitivity analysis and Bayesian framework could further be used to analyze and improve the predictability and parameterization of relatively coarse time step biogeochemistry models when the eddy flux and satellite data are available for other terrestrial ecosystems.

Citation: Tang, J., and Q. Zhuang (2009), A global sensitivity analysis and Bayesian inference framework for improving the parameter estimation and prediction of a process-based Terrestrial Ecosystem Model, *J. Geophys. Res.*, *114*, D15303, doi:10.1029/2009JD011724.

1. Introduction

[2] Large-scale process-based biogeochemistry models play an important role in providing more adequate estimates of global CO_2 budgets by integrating the information derived from empirical studies. To date, a number of models, such as the Terrestrial Ecosystem Model (TEM) [*Melillo et al.*, 1993; *Zhuang et al.*, 2003] and other models [*Running and Coughlan*, 1988; *Running and Hunt*, 1993; *VEMAP Members*, 1995; *Potter et al.*, 1993] have been developed and applied extensively. Those models usually make predictions by solving differential equations with parameters for representative ecosystem types. Such parameters are often obtained through model calibrations using observed annual data of C and nitrogen (N) pools and fluxes [e.g., *Raich et al.*, 1991; *McGuire et al.*, 1992]. The parameter values are determined when the simulated annual fluxes agree well with the observations at the site with some arbitrary criteria. However, as argued by *Thiemann et al.* [2001], a sound model calibration should be able to help reduce the uncertainty in parameterizations while the uncertainties in measured data and model structures (i.e., model formulations) are considered. Therefore a simple calibration technique by matching model output to observed data through manually tuning parameters may not be sufficient to reduce uncertainty of both parameters and model predictions. Further, simple calibration techniques may provide several sets of

[1]Purdue Climate Change Research Center, Purdue University, West Lafayette, Indiana, USA.
[2]Department of Earth and Atmospheric Sciences, Purdue University, West Lafayette, Indiana, USA.
[3]Department of Agronomy, Purdue University, West Lafayette, Indiana, USA.

0148-0227/09/2009JD011724$09.00

parameters for a single ecosystem, which allow the calibrated model to give similar predictions (so-called equifinality, see *Beven and Freer* [2001]), especially when the models are highly nonlinear. As a result, the calibrated parameters become another source of uncertainty in model predictions in addition to the incomplete understanding of ecosystem processes and underlying mechanisms in the models and the uncertainty in forcing data. Also, simple calibration techniques may not provide information on what data are essential to constrain the models, and they provide no guidance on what data should be collected in field experiments.

[3] To improve the parameterization and predictability of ecosystem models, good progress has been made using eddy flux data sets in a model-data fusion manner [e.g., *Braswell et al.*, 2005; *Williams et al.*, 2005; *Aalto et al.*, 2004; *Wang et al.*, 2001, 2007; *Santaren et al.*, 2007]. These studies often strive to constrain a few parameters of their models and these ecosystem models are mostly operated at finer time steps (e.g., hourly or daily). How the eddy flux data could be fused with coarse time step ecosystem models (e.g., monthly) using Bayesian approaches to constrain model parameter estimation and improve model predictability has not yet been well studied.

[4] Traditionally, the Bayesian inference technique can be implemented either iteratively or noniteratively. In the iterative way, the posterior at a time step is used as the prior for the next time step. The iterative methods include the Markov Chain Monte Carlo (MCMC) method [*Kuczera and Parent*, 1998; *Knorr and Kattge*, 2005], the Bayesian recursive method [*Gordon et al.*, 1993; *Thiemann et al.*, 2001; *Kaheil et al.*, 2006], and the gradient-based Bayesian inference method [*Santaren et al.*, 2007]. In these methods, the uncertainty of the parameters and prediction is reduced gradually as some convergence criteria are met or the maximum number of iterations is reached. However, in such methods, the Bayesian inference has to be coded into numerical models, so the inference procedure is not separated from the procedure of ecosystem model simulations. In contrast, the noniterative implementation of Bayesian inference is separated from the numerical model simulations [*Poole and Raftery*, 2000; *Hong et al.*, 2005], and the observational data are assimilated nonsequentially. Further, the noniterative way allows us to use different likelihood functions and different combinations of the observed and derived data in our Bayesian analysis without reconducting ecosystem model simulations.

[5] In this study, to demonstrate how eddy flux and satellite data could be used to improve the parameterization and predictability of a monthly time step process-based biogeochemistry model TEM, we developed a global sensitivity analysis and noniterative Bayesian inference framework. With the framework, we aimed to address the following questions: (1) How do TEM parameters affect the simulated seasonal C dynamics? (2) How do the parameters interact in influencing the overall model predictions? (3) How do the assumed error structures of the flux data affect the model parameterization and thus the overall model predictions? (4) How much uncertainty of parameters and model predictions can be reduced using the flux data with the developed model-data fusion technique? and (5) What flux data should be used to reduce the uncertainty of the model parameterization and predictions?

2. Methodology

[6] We developed a global sensitivity analysis and Bayesian inference framework and applied it to TEM for a black spruce ecosystem where the eddy flux data of carbon (C), water, and energy have been observed and derived [*Goulden et al.*, 1998; *Zhuang et al.*, 2001, 2002; *Clein et al.*, 2002; *Wofsy and Dunn*, 2001; *Dunn et al.*, 2007]. To improve the parameterization and predictability of TEM with the framework, we first defined the prior distributions for TEM parameters in controlling C and N processes, and ecosystem evapotranspirations (EET). We then conducted a set of Monte Carlo model simulations with the parameters sampled from the prior distributions using the Latin Hypercube Sampling technique (LHS [*Iman and Helton*, 1988]). A global sensitivity analysis with the first-order impact ratio (FOIR) was performed to rank key parameters of TEM [*Saltelli et al.*, 2004]. The interaction structures or correlations of TEM parameters conditioned on observational data were also examined with techniques described by *Ratto et al.* [2001]. Finally, we applied Bayesian inference on TEM parameters and model predictions with the MODIS GPP data from 2000 to 2006 [*Turner et al.*, 2006] and the observed or derived monthly eddy flux data. We used the 24 monthly data points from January 2003 to December 2004 from the site, which cover two complete annual cycles, for our Bayesian inference analysis. The remaining observed and derived data from 1994 to 2006 were then used to show the improvement in TEM simulations with the Bayesian inference technique, by comparing to conventional calibration methods [e.g., *Raich et al.*, 1991]. Below we first introduce parameters used in TEM and the study site. We then describe the details of our workflow and methods for the global sensitivity analysis and Bayesian inference (see Figure 1).

2.1. Description of the Terrestrial Ecosystem Model and the Study Site

[7] The Terrestrial Ecosystem Model (TEM) uses spatially referenced information on climate, elevation, soils, vegetation, and water availability to make monthly estimates of vegetation and soil C and N fluxes and pool sizes. The model is well documented and has been used to examine patterns of regional and global terrestrial C dynamics [e.g., *Raich et al.*, 1991; *McGuire et al.*, 1992, 2001; *Melillo et al.*, 1993; *Zhuang et al.*, 2001, 2002, 2003, 2004]. The version of TEM used in this study explicitly couples biogeochemical processes with the soil thermal dynamics of permafrost and nonpermafrost soils [e.g., *Zhuang et al.*, 2001, 2002, 2003, 2006; *Euskirchen et al.*, 2006; *Balshi et al.*, 2007]. We defined the net ecosystem production (NEP) used in TEM as the difference between the gross primary production (GPP) and the ecosystem respiration (RESP, the sum of autotrophic respiration, R_A, and heterotrophic respiration, R_H [*McGuire et al.*, 2001; *Zhuang et al.*, 2002, 2003]). These fluxes are influenced by changes in atmospheric CO_2, climate variability and change, the freeze-thaw status of the soil, disturbance history, and regrowth after disturbances.

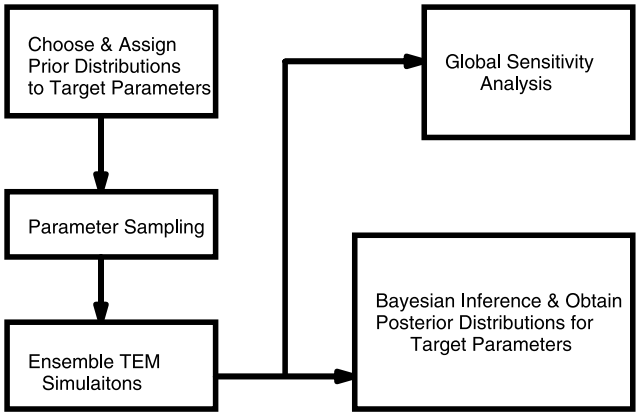

Figure 1. Flowchart of the global sensitivity analysis and Bayesian inference framework.

[8] In this study, we considered all TEM parameters related to C and N processes and EET for natural ecosystems and initial pool sizes of C and N in the vegetation and soils (see Table 1 [*Raich et al.*, 1991; *McGuire et al.*, 1992]). This could help identify which parameters are more important in determining carbon fluxes with our global sensitivity analysis, and which can be constrained using observational data with our Bayesian inference framework. We excluded the parameters related to the soil thermal module in this version of TEM, using their values from our previous study [*Zhuang et al.*, 2003]. Our analyses were conducted for a mature black spruce ecosystem in the Northern Study Area of NASA's Boreal Ecosystem-Atmosphere Study (BOREAS [*Sellers et al.*, 1997; *Dunn et al.*, 2007]), which is located at 55.88°N, 98.48°W, in central Manitoba, Canada. The conventional calibration was also conducted to provide base values of the parameters for comparison. Specifically, in the conventional calibration, we ran TEM continuously with long-term average climate data and an atmospheric CO_2 concentration of 340 ppmv. The parameter values were changed manually until the simulated fluxes and pool sizes matched the field data with a certain tolerance (e.g., 1%), and the obtained parameter values were then considered as optimal for the site. Three criteria were used to judge the success of conventional calibration: (1) the modeled annual NPP and GPP match the observations; (2) the annual nitrogen uptake is close to observations; and (3) the annual NEP converges to nearly zero with the prescribed tolerance (e.g., 1% [see *Zhuang et al.*, 2001; *Clein et al.*, 2002, for details]). For the Bayesian inference, the prior distributions for these parameters were assumed uniform with lower and upper bounds obtained either from literature review or from our previous studies (see Table 1). Based on the prior samples generated from LHS sampling, a set of 500,000 (a number determined by experience) Monte Carlo ensemble TEM simulations was conducted for the ecosystem from 1975 to 2006. The driving climate data, developed from the meteorological station at nearby Thompson Airport, Manitoba (around 50 km away from the site), were obtained from the Canadian National Climate Data and Information Archive (http://climate.weatheroffice.ec.gc.ca/climateData/canada_e.html). Soils and elevation data derived from our previous study were used to drive TEM simulations at the site [*Zhuang et al.*, 2002; *Clein et al.*, 2002]. The Bayesian inference analyses were conditioned on different combinations of the measured eddy flux NEP data, the derived RESP data, and the MODIS GPP and EET data. The EET was based on latent heat measurements. The monthly NEP and EET data were aggregated from half-hourly measurements. The RESP data were obtained with a regression method based on measured nighttime NEP and local climate data. The derived GPP data were calculated as the sum of NEP and RESP [*Goulden et al.*, 1997], and were only used for validation of the results from the Bayesian inference analysis. To obtain independent GPP data from eddy flux data for the Bayesian inference, we used the 1 km × 1 km GPP derived from the MODIS (Moderate Resolution Imaging Spectroradiometer) sensor [*Running et al.*, 2004]. We first selected the 1 km × 1 km grid cell that covers the tower (at 55.88007°N, 98.48139°W) where the carbon and water fluxes were measured for the black spruce ecosystems used in this study. We then aggregated the GPP for the grid cell using 8-day temporal resolution GPP data for the period from 2000 to 2006 to obtain monthly GPP. Compared to the derived GPP from eddy flux measurements, the satellite-based data overestimated GPP in the middle of the growing season (from May to August), and underestimated GPP near the onset (late April and early May) and senescence (September) of the growing season in our study period. Overall, the MODIS GPP has a linear fitting $y = 0.83x + 4.60$ (g C m^{-2} mon^{-1}), $R^2 = 0.95$ ($p < 0.001$), with x being the MODIS GPP and y the GPP flux measurement.

2.2. Global Sensitivity Analysis and Bayesian Inference Framework

[9] Our framework was based on Bayes' theorem:

$$\Pr(\boldsymbol{\theta}|\mathbf{V}) \propto \Pr(\mathbf{V}|\boldsymbol{\theta}) \Pr(\boldsymbol{\theta}) \quad (1)$$

where $\Pr(\boldsymbol{\theta}|\mathbf{V})$ is the posterior after Bayesian inference conditioned on available observations $\mathbf{V}$ (hereafter the bold letter indicates a matrix). $\boldsymbol{\theta}$ is the matrix of parameters and TEM outputs (e.g., GPP) and $\mathbf{V}$ is the matrix of observation or the matrix of the differences between prior simulations and the corresponding observations, whose element V_{ij} denotes the type j data $V_{(\cdot)j}$ at time step i. $\Pr(\mathbf{V}|\boldsymbol{\theta})$ is the likelihood function, which will be calculated as a function of TEM Monte Carlo simulations and the available eddy flux data. $\Pr(\boldsymbol{\theta})$ is the prior of the TEM parameters and our estimated C fluxes (e.g., GPP, RESP and NEP) and EET.

[10] To address our research questions, we first conducted TEM ensemble simulations with parameter priors. Second, the likelihood function $\Pr(\mathbf{V}|\boldsymbol{\theta})$ was calculated based on model simulations and observations. Third, the global sensitivity analysis was applied, and fourth, the Bayesian inference was conducted. Below we detail each step (Figure 1).

2.2.1. The Prior Monte Carlo Simulations

[11] Monte Carlo TEM simulations were conducted based on the prior distributions of parameters to provide C fluxes for the global sensitivity analysis and Bayesian inference analysis. The prior distributions of TEM parameters were assumed with uniform shapes (Table 1). Initial parameter value ranges were assigned based on either literature review or estimates. These parameters are related to (1) initial pools

Table 1. TEM Parameters Involved in This Study[a]

ID	Acronym	Definition	Prior Range	Units	Reference
			Initial Pool Sizes		
1	C_s	Initial organic C in soil and detritus	[6000, 20,000]	g m^{-2}	*McGuire et al.* [1992] and *O'Neill et al.* [2003]
2	C_v	Initial organic C in vegetation	[2000, 20,000]	g m^{-2}	*McGuire et al.* [1992] and *O'Neill et al.* [2003]
3	N_{av}	Available inorganic N in soil and detritus	[0.1, 0.9]	g m^{-2}	*McGuire et al.* [1992] and *Weber and Van Cleve* [1984]
4	N_s	Initial organic N in soil and detritus	[250, 1000]	g m^{-2}	*McGuire et al.* [1992] and *Van Cleve et al.* [1983]
5	N_v	Initial N in vegetation	[10, 40]	g m^{-2}	*McGuire et al.* [1992] and *Van Cleve et al.* [1983]
			Soil Texture Properties		
6	$P_{orosity}$	Soil porosity	[30, 60]	cm^3 cm^{-3}	*Frolking et al.* [1996]
7	F_{ldcap}	Soil field capacity	[25, 40]	cm^3 cm^{-3}	*Frolking et al.* [1996]
8	W_{iltpt}	Soil wilting point	[20, 25]	cm^3 cm^{-3}	*Frolking et al.* [1996]
			Vegetation Parameters		
9	R_{ootz}	Effective rooting depth	[0.7, 2.5]	M	Guess based on conventional calibration
10	k_c	Half saturation constant for CO_2-C uptake by plants	[20, 600]	μL L^{-1}	*Raich et al.* [1991]
11	k_l	Half saturation constant for PAR use by plants	[20, 600]	μL L^{-1}	*Raich et al.* [1991]
12	T_{min}	Minimum temperature for GPP	[−12, −1]	°C	Guess based on conventional calibration
13	T_{optmin}	Minimum optimum temperature for GPP	[0, 15]	°C	Guess based on conventional calibration
14	T_{optmax}	Maximum optimum temperature for GPP	[15, 25]	°C	Guess based on conventional calibration
15	T_{max}	Maximum temperature for GPP	[25, 35]	°C	Guess based on conventional calibration
16	RAQ10A0	Leading coefficient of the Q10 model for plant respiration	[1.3502, 3.3633]	None	Guess based on conventional calibration
17	RAQ10A1	First order coefficient of the Q10 model for plant respiration	[−0.054577, −0.051183]	$°C^{-1}$	Guess based on conventional calibration
18	RAQ10A2	Second order coefficient of the Q10 model for plant respiration	[0.0022902, 0.0024381]	$°C^{-2}$	Guess based on conventional calibration
19	RAQ10A3	Third order coefficient of the Q10 model for plant respiration	[−0.0000417, −0.0000397]	$°C^{-3}$	Guess based on conventional calibration
20	k_{n1}	Half saturation constant for N uptake by vegetation	[0.5, 10]	g m^{-3}	*Raich et al.* [1991]
21	k_{n2}	Half saturation constant for N uptake by heterotrophic organisms	[0.5, 10]	g m^{-3}	*Raich et al.* [1991]
22	MINLEAF	Minimum photosynthetic capacity of vegetation	[0.2, 0.8]	None	*McGuire et al.* [1992]
23	ALEAF	Coefficient to model the relative photosynthetic capacity of vegetation	[0.1, 1.0]	None	*McGuire et al.* [1992]
24	BLEAF	Coefficient to model the relative photosynthetic capacity of vegetation	[0.1, 1.0]	None	*McGuire et al.* [1992]
25	CLEAF	Coefficient to model the relative photosynthetic capacity of vegetation	[0.0, 0.5]	None	*McGuire et al.* [1992]
26	MOISTOPT	Optimum soil moisture content for R_H	[20, 80]	%	*McGuire et al.* [1992]
27	RHQ10	Change in R_H rate due to 10°C temperature increase	[1, 3]	None	*Raich et al.* [1991]
28	CMAX	Maximum rate of photosynthesis C	[50, 1500]	g m^{-2} mo^{-1}	*McGuire et al.* [1992]
29	CFALL	Proportion of vegetation carbon loss as litterfall monthly	[0.0001, 0.015]	g g^{-1} mo^{-1}	Guess based on conventional calibration
30	KRC	Logarithm of plant respiration rate at 0°C	[−7.5, −1.5]	None	*McGuire et al.* [1992]
31	KDC	Heterotrophic respiration rate at 0°C	[0.0005, 0.007]	g g^{-1} mo^{-1}	*McGuire et al.* [1992]
32	NMAX	Maximum rate of N uptake by vegetation	[0.05, 0.7]	g m^{-2} mo^{-1}	*McGuire et al.* [1992]
33	NFALL	Proportion of vegetation nitrogen loss as litter-fall monthly	[0.003, 0.012]	g g^{-1} mo^{-1}	*McGuire et al.* [1992]
34	NUP	Ratio between N immobilized and C respired by heterotrophs	[0.005, 0.1]	g g^{-1}	*McGuire et al.* [1992]
35	VEGC2N	Mean C:N of vegetation	[200, 600]	g g^{-1}	Guessed based on conventional calibration

[a]All a priori is assumed with uniform distributions.

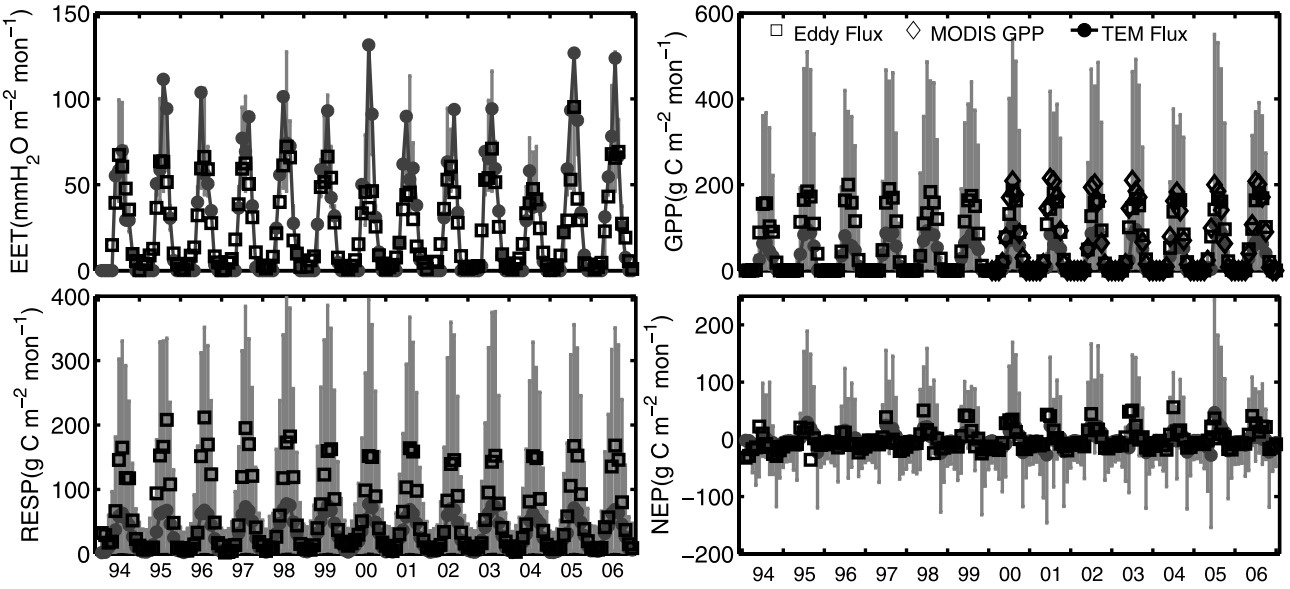

Figure 2. TEM simulations before applying the Bayesian inference framework. 500,000 sets of parameters were used to compose the above results. The error bar denotes the 95% credible interval or confidence interval of the simulated fluxes at that month; the gray solid line is the value at the 50% confidence level.

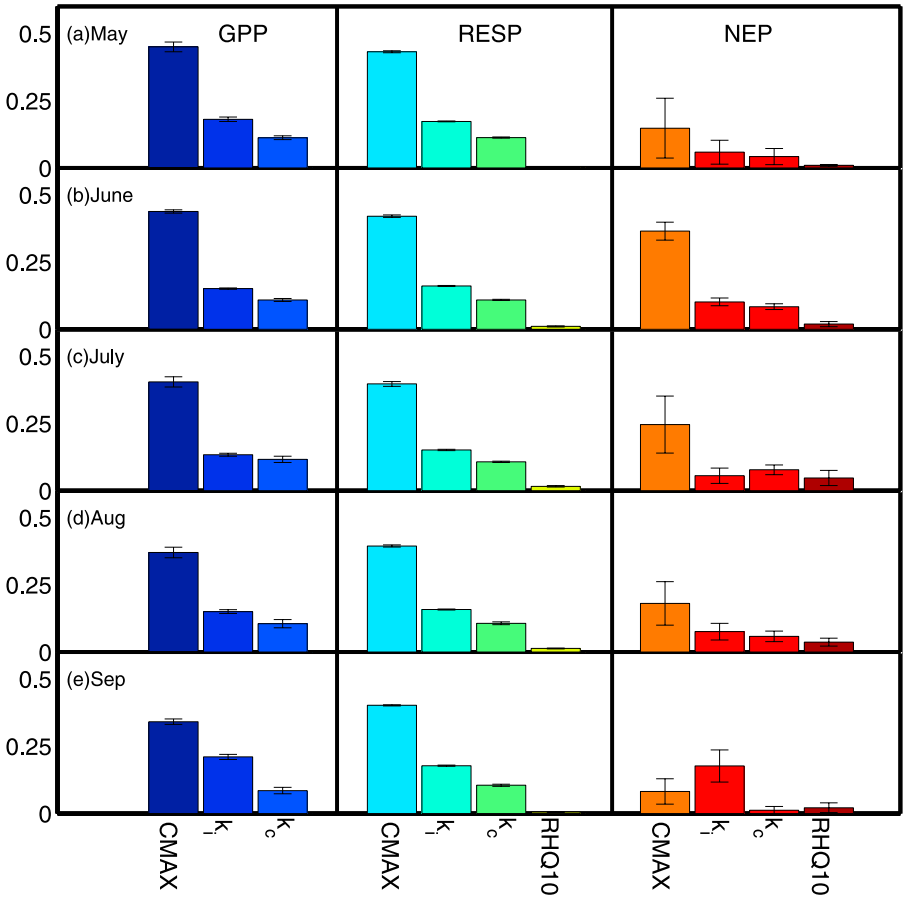

Figure 3. The first-order impact ratios (FOIRs) for the most influential parameters for the three C fluxes (GPP, RESP, and NEP) during the growing season (10-year average of 1988–1997) in (a) May, (b) June, (c) July, (d) August, and (e) September. The error bar denotes the standard deviation deduced using the bootstrap method.

Table 2. Ranks of the First-Order Impact Ratios (FOIRs) for Different Annual Carbon Fluxes[a]

Acronym	GPP	RESP	NEP
CMAX	**1**	**1**	**1**
k_l	**2**	**2**	**2**
k_c	**3**	**3**	**3**
T_{min}	*4*	16	*8*
CFALL	*5*	*5*	*5*
k_{n2}	*6*	*7*	*7*
MINLEAF	7	17	17
ALEAF	8	13	18
BLEAF	9	15	*11*
NMAX	10	*9*	*12*
F_{ldcap}	11	21	*9*
NUP	12	10	13
NFALL	13	11	16
k_{n1}	14	12	15
CLEAF	15	14	19
R_{ootz}	16	19	14
RAQ10A0	17	*8*	*10*
KRC	18	*6*	*6*
KDC	19	22	21
T_{max}	20	23	24
VEGC2N	21	18	23
W_{iltpt}	22	27	22
RHQ10	23	**4**	**4**
MOISTOPT	24	20	20
T_{optmin}	25	25	26
T_{optmax}	26	24	25
$P_{orosity}$	27	29	31
N_s	28	26	27
RAQ10A1	29	28	29
RAQ10A3	30	31	30
RAQ10A2	31	34	34
N_{av}	32	32	33
C_v	33	30	28
N_v	34	33	32
C_s	35	35	35

[a]The impact ratios in bold are greater than 5%, those in italics are between 0.5% and 5%, and the rest are below 0.5%.

of C and N; (2) process parameters of C and N fluxes; and (3) process parameters of EET. We used the LHS algorithms [*Iman and Helton*, 1988] to generate parameter samples for the TEM Monte Carlo simulations. The LHS draws n samples for k random variables $\theta_1, \ldots, \theta_k$ over the feasible space described by their probability distributions. Sampling was conducted in three steps: (1) each variable was divided into n nonoverlapping intervals on the basis of equal probability in terms of the cumulative distribution function; (2) one value from each interval was selected randomly with respect to the probability density in the interval; and (3) the n values obtained for θ_1 were randomly paired with the n values of θ_2. Then these n pairs were further randomly paired with the n values of θ_3 to form n triplets and so forth, until n sets of k-tuples are formed. These n sets of parameters were used to drive the TEM for Monte Carlo simulations. In this study, we did not incorporate correlations among the parameters for their prior samples, but, if available, they can be incorporated into the samples through the Spearman rank correlation matrix at step (3) [e.g., see *Iman and Conover*, 1982].

2.2.2. Calculation of Likelihood Function

[12] To calculate the likelihood function ($\Pr(\mathbf{V}|\boldsymbol{\theta})$) in equation (1), following other studies [*Hong et al.*, 2005; *Santaren et al.*, 2007], we assumed the monthly flux data are statistically independent from month-to-month and from one flux type to another. We also assumed that the observed and derived data obey the following error distribution [*Thiemann et al.*, 2001]:

$$p_i(v_{ti}|\sigma_{ti},\beta_i,\theta) = \omega(\beta_i)\sigma_{ti}^{-1}\exp\lfloor -c(\beta_i)|v_{ti}/\sigma_{ti}|^{2/(1+\beta_i)}\rfloor \quad (2)$$

[13] Such an error distribution allowed us to examine the effects of different error structures on Bayesian inference results, using different specified values of $\beta_i \in (-1, 1]$. For example, equation (2) is a normal distribution when $\beta_i = 0$. It is a double exponential distribution when $\beta_i = 1$. It tends to be a uniform distribution as β_i approaches -1. $i = 1, \ldots, N$ are labels for different types of data. Variations σ_{ti}^2 were assumed as constant during the time period of $t_{i-1} < t \le t_i$. $c(\beta_i)$ $c(\beta_i)$ and $\omega(\beta_i)$ are defined as:

$$c(\beta_i) = \left\{\frac{\Gamma[3(1+\beta_i)/2]}{\Gamma[(1+\beta_i)/2]}\right\}^{1/(1+\beta_i)} \quad (3)$$

and

$$\omega(\beta_i) = \frac{\{\Gamma[3(1+\beta_i)/2]\}^{1/2}}{(1+\beta_i)\{\Gamma[(1+\beta_i)/2]\}^{3/2}} \quad (4)$$

[14] We further assumed TEM outputs follow the error distribution defined by equation (2) in the logarithmic space. Thus we had:

$$p(\mathbf{V}|\boldsymbol{\sigma},\boldsymbol{\beta},\boldsymbol{\theta}) = \prod_{i=1}^{N}\prod_{t=1}^{T}\omega(\beta_i)\sigma_{ti}^{-1}\exp\left[-c(\beta_i)|v_{ti}/\sigma_{ti}|^{2/(1+\beta_i)}\right] \propto \exp\left[-\sum_{i=1}^{N}c(\beta_i)\sum_{t=1}^{T}|v_{ti}/\sigma_{ti}|^{2/(1+\beta_i)}\right] \quad (5)$$

where $\boldsymbol{\sigma} = \{\sigma_{ti}\}$ and $\mathbf{V} = \{v_{ti}\}$ are matrices with a size of $T \times N$, and $\boldsymbol{\beta} = \{\beta_i\}$ is a vector with size of N. Further, we assumed σ_{ti} are constant (equals to σ_i) during the period of $0 < t \le T$ after the implementation of some variable transformations, such as the logarithm transformation we assumed. We then used the Jeffery's prior $p(\sigma_{ti}) = 1/\sigma_i$, $\sigma_i > 0$ [*Box and Tiao*, 1973] and summed up the effect of σ_{ti}, which was accomplished by defining a new integration variable $x_{ti} = v_{ti}/\sigma_{ti}$ in equation (5) and

Table 3. Sum of All FOIRs for the Three C Fluxes Simulated With TEM During the Growing Season[a]

	GPP	RESP	NEP
May	0.81 ± 0.018	0.79 ± 0.005	0.46 ± 0.122
June	0.77 ± 0.006	0.77 ± 0.003	0.67 ± 0.031
July	0.74 ± 0.009	0.76 ± 0.005	0.59 ± 0.070
August	0.73 ± 0.010	0.76 ± 0.003	0.55 ± 0.055
September	0.73 ± 0.007	0.76 ± 0.003	0.50 ± 0.050

[a]Values are given in the form of mean ± 1 standard deviation.

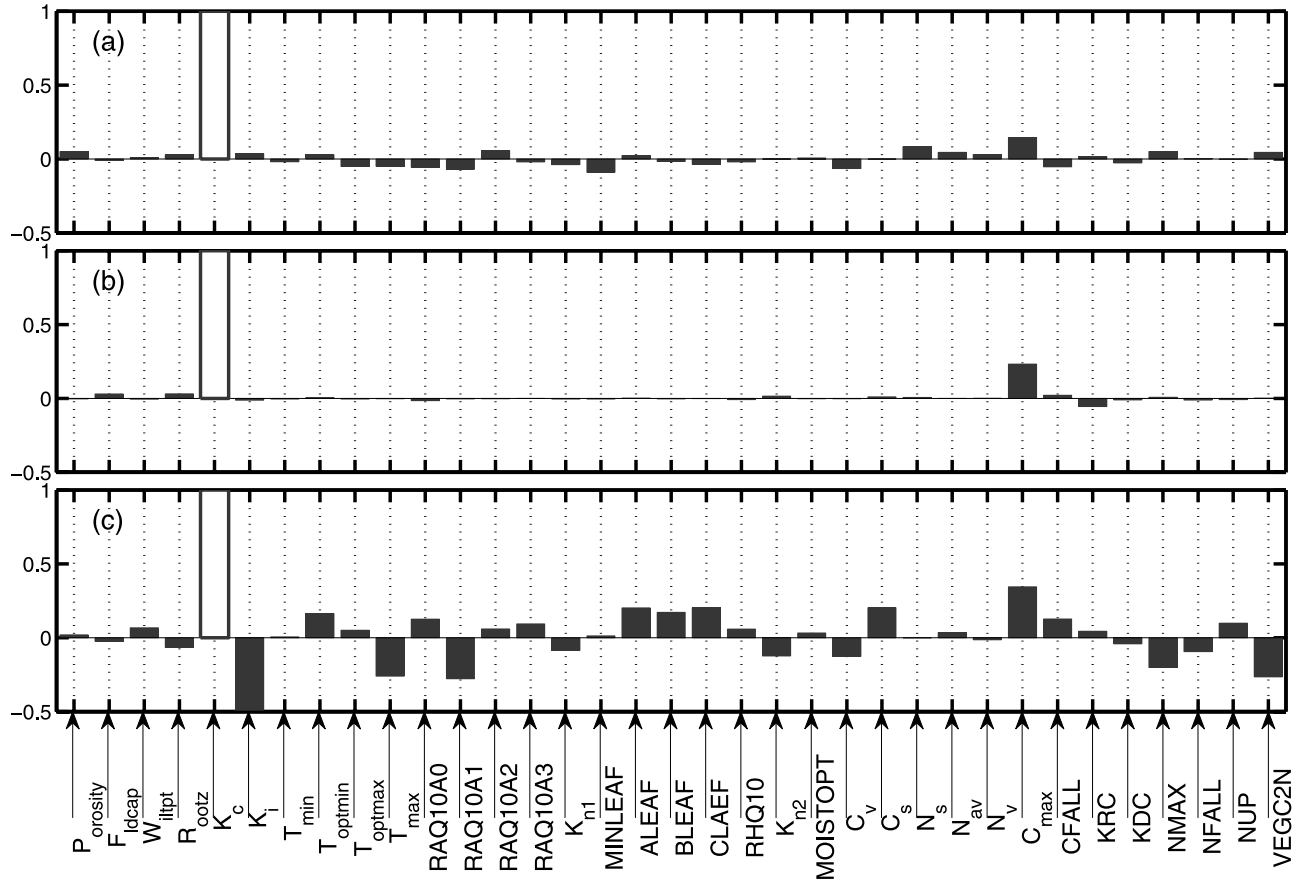

Figure 4. Plot of interaction structure of k_c against all other parameters when conditioned on different combination of flux data (a) EET and MODIS GPP; (b) EET and NEP; and (c) EET, MODIS GPP, and NEP. $\beta_i = 0$ (i.e. normal error distribution) was used throughout the computation. Data points from January 2003 to December 2004 were used to show interaction structures of TEM parameters.

integrating against x_{ti} from zero to infinity to obtain the likelihood function:

$$p(\mathbf{V}|\boldsymbol{\beta},\boldsymbol{\theta}) = \frac{1}{2^N}\prod_{i=1}^{N}\Gamma\left[(1+\beta_i)\left(T-\frac{1}{2}\right)\right][\omega(\beta_i)]^T \cdot\left[c(\beta_i)\sum_{t=0}^{T}|v_{ti}|^{2/(1+\beta_i)}\right]^{(1/2-T)(1+\beta_i)} \propto \prod_{i=1}^{N}\left[\sum_{t=1}^{T}|v_{ti}|^{2/(1+\beta_i)}\right]^{(1/2-T)(1+\beta_i)} \quad (6)$$

[15] We used the term after the symbol $\propto$ in equation (6) as the likelihood function throughout this study.

2.2.3. Global Sensitivity Analysis

[16] Based on prior TEM ensemble simulations and likelihood calculations, the global sensitivity analysis was conducted to (1) identify the key parameters in determining C fluxes with the first-order impact ratio (FOIR) and (2) examine the interaction structures among TEM parameters. Such an analysis also helps explain the importance of partitioning NEP measurements into GPP and RESP in order to constrain the TEM simulations with the Bayesian inference technique. The credible intervals or confidence intervals for fluxes simulated by TEM with prior parameter samples were also presented by values at statistical levels 2.5% and 97.5%.

[17] The FOIR is defined as:

$$I_k = \frac{\mathrm{Var}(E[Y|\theta_k])}{\mathrm{Var}(Y)} \quad (7)$$

where I_k states how much variance of the output Y is contributed by the kth parameter θ_k, or, how much uncertainty in the output would be reduced, in the first-order approximation, by fixing the parameter θ_k at its true value [*Saltelli et al.*, 2004]. For a nonlinear model, the sum of I_k for all parameters will usually be less than 1.0 due to possible interactions among parameters. Therefore the sum of all I_k can also be used to indicate how important the interactions among parameters are in contributing to the uncertainty of the model output. We calculated the FOIR using the simulated monthly and annual GPP, RESP and NEP during the growing season from May to September [*Clein et al.*, 2002] with a 10-year average from 1988 to 1997. The 10-year average smoothing was employed to remove modulations due to interannual climate variability. The uncertainties of FOIRs were estimated with the bootstrap method [*Davison and Hinkley*, 1997].

Table 4. TEM Parameter Values at Different Statistical Levels After Bayesian Inference, Conditioned on EET, MODIS GPP, and NEP Data With $\beta_i = 0$

Acronym	Base Value[a]	Posterior 2.5%	Posterior 50%	Posterior 97.5%	Statistical Mode[b]	Parameter Class[c]
			Initial Pool Sizes			
C_s	12791.1	6329.080	12540.700	19674.600	16262.300	PC
C_v	9006.52	2287.590	8761.220	19657.500	2287.590	EH
N_{av}	0.16125	0.130723	0.434495	0.885501	0.406843	PC
N_s	527.72	260.469	661.564	972.342	665.901	PC
N_v	30.044	10.622	26.617	38.927	24.031	PC
			Soil Texture Properties			
$P_{orosity}$	54	30.8008	43.9686	58.0861	52.5254	PC
F_{ldcap}	34.58	25.3488	30.5547	39.4260	27.7920	PC
W_{iltpt}	21.5875	20.1166	22.3403	24.8450	23.1154	PC
			Vegetation Parameters			
R_{ootz}	2.3977	1.5885	1.8264	2.4041	1.8283	WC
k_c	100	23.6180	144.0210	473.0020	466.9930	PC
k_l	75	23.9540	124.4270	503.8300	24.7819	EH
T_{min}	−8.0	−8.8810	−3.2604	−1.1644	−3.2604	WC
T_{optmin}	5.5	0.9889	8.3278	14.4576	12.9523	PC
T_{optmax}	20.0	15.3681	20.5690	24.8717	23.1597	PC
T_{max}	29.0	25.1608	29.4578	34.8365	25.2474	EH
RAQ10A0	2.35665	1.9357	2.8443	3.3448	2.9422	WC
RAQ10A1	−0.053077	−0.054452	−0.052801	−0.051206	−0.053454	PC
RAQ10A2	0.0023842	0.002294	0.002361	0.002436	0.002372	PC
RAQ10A3	−0.00004110	−0.000042	−0.000041	−0.000040	−0.000040	EH
k_{n1}	4.2	1.333	6.529	9.835	6.925	PC
k_{n2}	4.2	0.684	4.155	9.807	2.142	PC
MINLEAF	0.5	0.2332	0.4938	0.9751	0.5409	PC
ALEAF	0.42893	0.11847	0.49348	0.97255	0.92480	PC
BLEAF	0.33295	0.11483	0.38680	0.92465	0.41803	PC
CLEAF	0.32228	0.02992	0.27364	0.49645	0.35742	PC
MOISTOPT	0.5	0.2070	0.5073	0.7789	0.5187	PC
RHQ10	2.0	1.1027	2.3541	2.8599	2.4120	WC
CMAX	768.07	683.76	1185.95	1480.55	1351.57	WC
CFALL	0.002037	0.000141	0.002861	0.011826	0.005423	EH
KRC	−6.467	−7.191340	−5.213690	−3.140830	−4.382210	PC
KDC	0.00216527	0.000935	0.003744	0.006763	0.002847	WC
NMAX	0.374677	0.0516254	0.2858710	0.672993	0.2102410	PC
NFALL	0.007955	0.003192	0.007544	0.011723	0.006800	PC
NUP	29.2639	13.974000	68.446300	97.392000	93.683800	PC
VEGC2N	375.0	207.0490	372.7000	576.2950	207.0490	EH

[a]The base values of the TEM parameters are obtained from conventional calibration.
[b]The statistical mode values are TEM parameter values corresponding to the maximum posteriori for the black spruce site in this study.
[c]For the parameter classification, WC means well-constrained parameters, PC means poorly constrained parameters, and EH means edge-hitting parameters.

[18] Using a similar method described by *Ratto et al.* [2001], we analyzed the interaction structure among the parameters of TEM with the following steps:

[19] (1) Normalizing the likelihood function such that:

$$\sum_{s=1}^{NS} \omega_s(\mathbf{V}|\beta,\theta) = 1 \tag{8}$$

where *NS* is the number of TEM Monte Carlo simulations, which was 500,000 in this study. **V** denotes the differences between the simulated and observed fluxes, and β, θ are parameters of TEM and the likelihood function, respectively. This step reassigns the probability to different sample points in the parameter space according to the difference between the simulated and measured or derived eddy fluxes. The sample point with a smaller difference will receive a higher probability or weight.

[20] (2) Calculating the first- and the second-order moments for all model parameters:

$$\hat{E}(\theta_k) = \sum_{s=1}^{s=NS} \theta_{k,s}\ \omega_s(\mathbf{V}|\beta,\theta) = \hat{\mu}_k \tag{9}$$

$$\hat{V}(\theta_k) = \sum_{s=1}^{s=NS} \theta_{k,s}^2\ \omega_s(\mathbf{V}|\beta,\theta) - \hat{\mu}_k^2 = \hat{\sigma}_k^2 \tag{10}$$

[21] (3) Rescaling the input parameters (i.e., parameters in Table 1):

$$\tilde{\theta}_k = \frac{\theta_k - \hat{\mu}_k}{\hat{\sigma}_k} \tag{11}$$

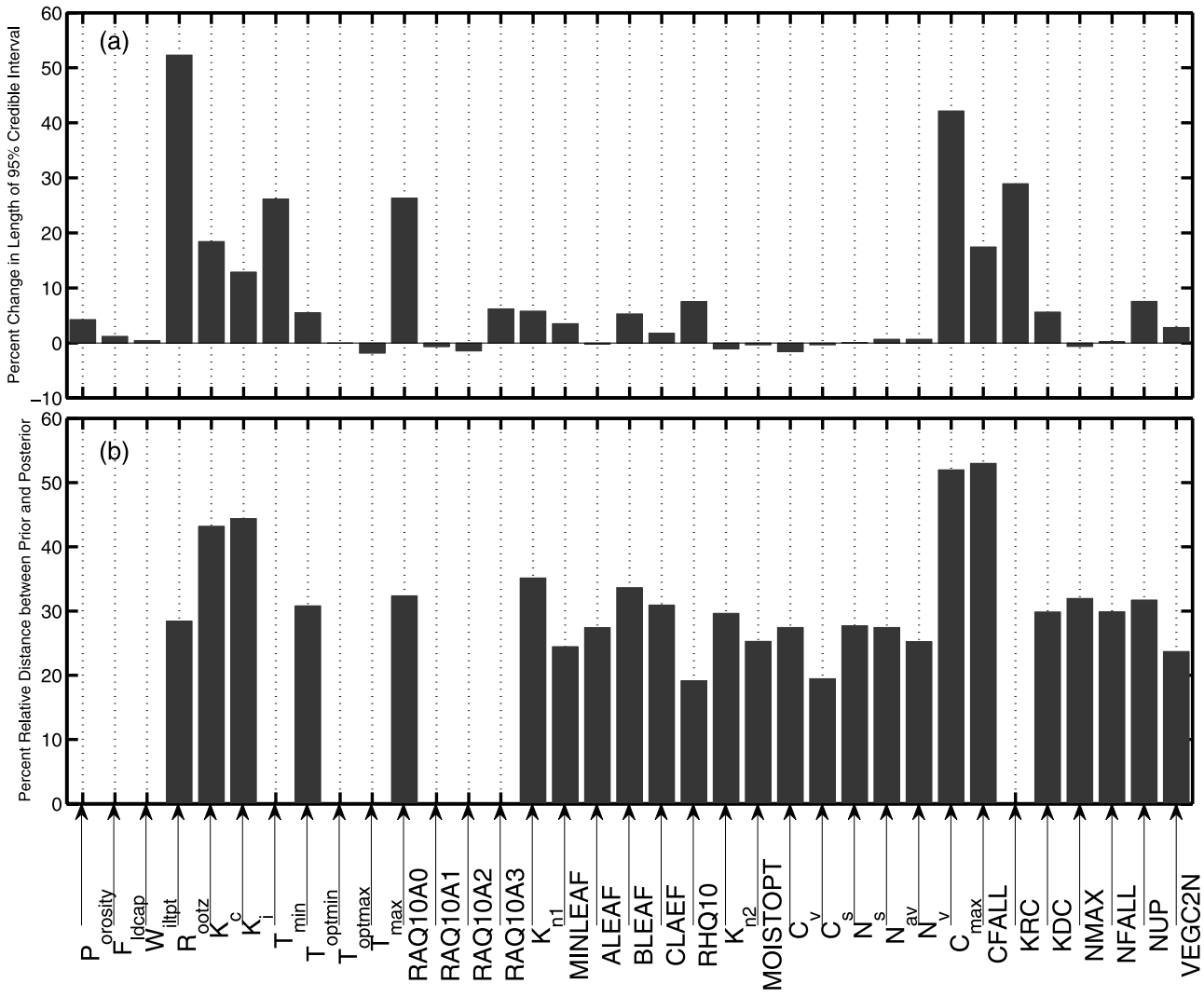

Figure 5. (a) Percentage change in the length of 95% credible interval after Bayesian inference when compared to the prior marginal distributions. Zero or negative values indicate that no information is extracted from the eddy flux data using Bayesian inference for the parameter. (b) Percentage change of the relative distance for a parameter's distribution after Bayesian inference compared to its prior.

[22] (4) Computing the correlation coefficient among parameters (e.g., *k*th and *j*th parameter):

$$\hat{\rho}_{k,j} = \sum_{s=1}^{s=NS} \widetilde{\theta}_{k,s}\ \widetilde{\theta}_{j,s}\ \omega_s(\mathbf{V}|\beta,\theta) \in [-1,1] \tag{12}$$

[23] We calculated the interaction structures among TEM parameters conditioned on the observed or derived data of (1) EET and MODIS GPP; (2) EET and NEP, and (3) EET, MODIS GPP and NEP, respectively. We applied the following rules to interpret our results: If two parameters are positively correlated, then these two parameters act as a quotient/difference effect when driving the response variable in the model. That means, when one parameter increases its value, another parameter also has to increase in order to have the same effects on the response variable associated with these two parameters. If two parameters are negatively correlated, then the two parameters act as a product/sum effect, which means that the values of two parameters should be changed in opposite directions to maintain the same effects on a response variable.

[24] The 500,000 sets of simulated C fluxes and EET based on prior parameter samples were analyzed to estimate the 95% credible intervals (i.e., intervals confined between values at 2.5% and 97.5% statistical levels, as defined conventionally) of the fluxes of EET, GPP, RESP, and NEP (see Figure 2, denoted by error bounds). Also estimated are median values at the 50% statistical level.

2.2.4. Bayesian Inference on Model Parameters and Prediction

[25] With the outputs from Monte Carlo simulations, and the well-defined likelihood function equation (6), the Bayesian inference defined by equation (1) can be implemented to make inference on our chosen TEM parameters and the simulated C fluxes and EET. We employed the Sampling Importance Resampling (SIR) algorithm by *Skare et al.* [2003] to construct the posterior distributions for both model parameters and modeled fluxes with following steps:

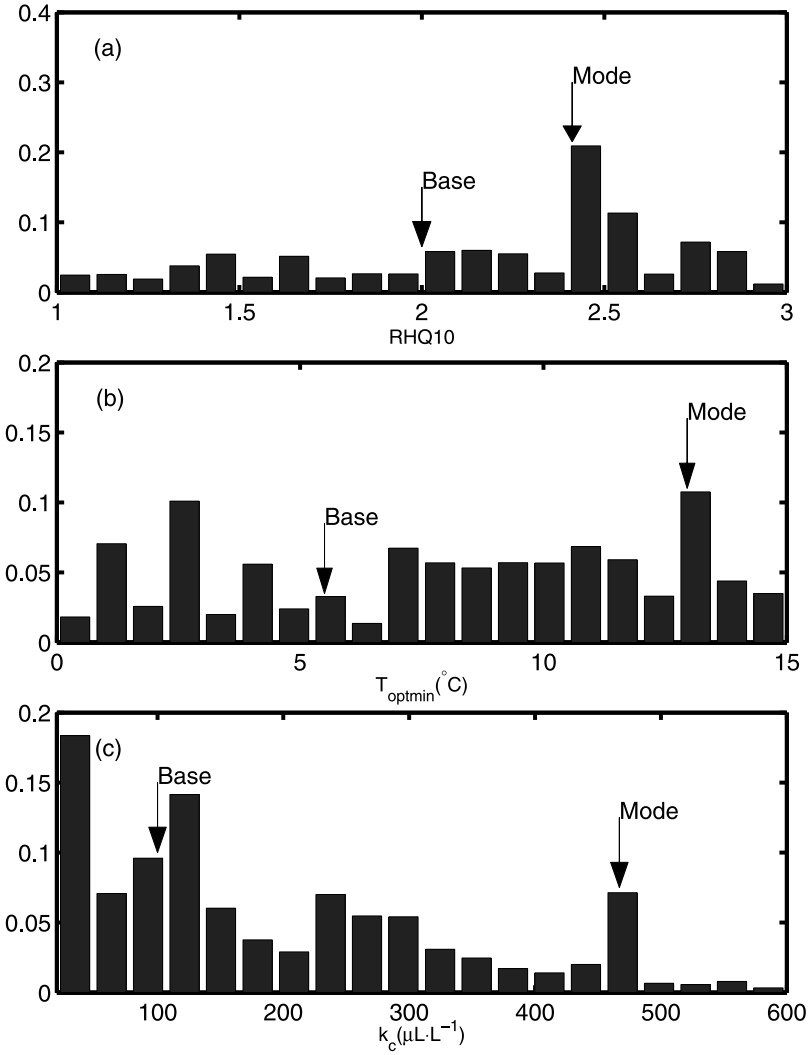

Figure 6. The normalized frequency plots for RHQ10, T_{optmin} and k_c, which are corresponding to (a) well-constrained (WC), (b) poorly constrained (PC), and (c) edge-hitting (EH) parameters, respectively. The mode values are corresponding to the set of parameters which have the highest value of the likelihood function in the ensemble simulation. The base values were obtained from the conventional calibration.

[26] (1) Computing the importance ratio $h(\boldsymbol{\theta_j}) = p(\boldsymbol{\theta_j}|\mathbf{V})/p(\boldsymbol{\theta_j})$, using equation (6) for each sample, so that a vector of length 500,000 is formed. In this study, with the uniform prior, the importance ratio is just the value of likelihood function.

[27] (2) Let $S_{-j} = \sum_{i \neq j} h(\boldsymbol{\theta}_i)$ be the sum of all importance ratios excluding $h(\boldsymbol{\theta}_j)$.

[28] (3) For $k = 1, \ldots, m$, draw parameter samples j_k with probability q_{j_k} from the 500,000 samples, where $q_j \propto h(\boldsymbol{\theta}_j)/S_{-j}$. We used the Probability Proportional to Size (PPS) sampling technique [*Hong et al.*, 2005] to draw the samples. The resampling was done with replacement.

[29] (4) For the picked j_k, get the corresponding $\boldsymbol{\theta}_{j_k}$, $k = 1, \ldots, m$. In our analysis, we set $m = 50{,}000$. This number was chosen according to the suggestion that, to produce stable results, setting the ratio of prior sample size to posterior sample size as 10 is appropriate [*Green et al.*, 1999; *Bates et al.*, 2000].

[30] In step (2), $i = j$ is removed to reduce the correlation between the modifying factor Z_j, which is conventionally used to define $q_j \propto h(\theta_j)/Z_j = h(\theta_j)/\sum h(\theta_j)$, and the importance ratio $h(\theta_j)$, from $corr\{h(\theta_j), Z_j\} = corr\{h(\theta_j), \sum h(\theta_j)\} =$ (1) to $corr\{h(\theta_j), Z_j\} = corr\{h(\theta_j), S_{-j}\} = O(1/n)$, so that elements with higher importance ratio are more easily drawn in SIR.

[31] Using the NEP flux data only, the parameters related to C dynamics of biogeochemistry models operated at daily time step or even finer time steps could be well constrained with Bayesian inference techniques [e.g., *Santaren et al.*, 2007]. However, this may not be the case for monthly time step biogeochemistry models, such as TEM, since the monthly NEP data obtained by aggregating measurements at finer timescales contain less information than the original data. Thus to make recommendations for the C fluxes to be measured and derived to improve parameter estimations for TEM, rather than just using NEP fluxes, we conducted Bayesian inference analyses conditioned on different com-

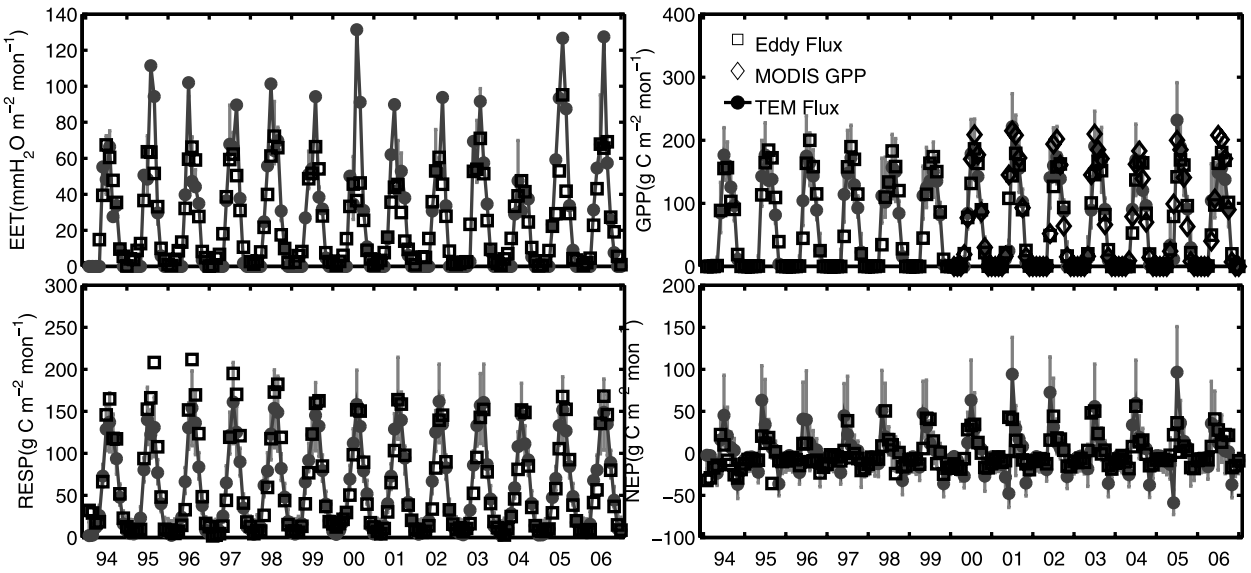

Figure 7. The posterior TEM outputs after Bayesian inference with a normal error distribution ($\beta_i = 0$). The error bar denotes the 95% credible interval of the variables in that month; the gray solid time series are the median values at the 50% confidence level after the Bayesian inference. The data points from January 2003 to December 2004 were used in Bayesian conditioning; the rest of data, including the derived GPP from April 1994 to December 2006 were used for verification.

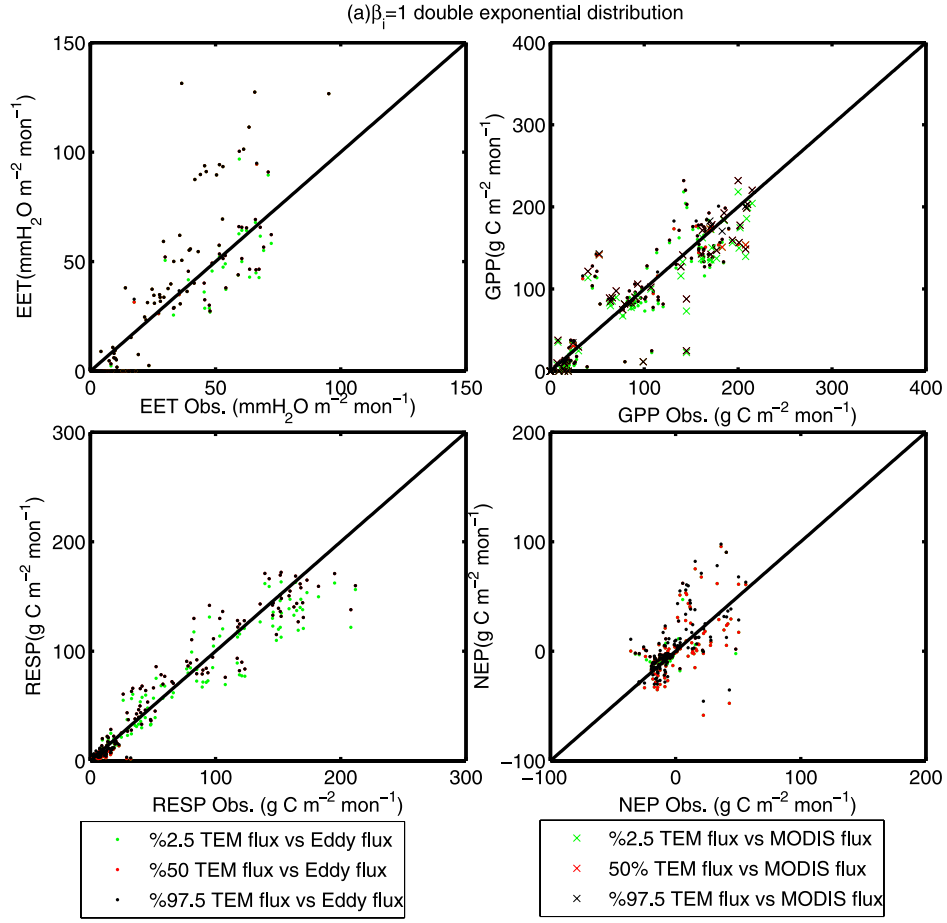

Figure 8a. Scatterplots of the posterior TEM outputs against observations after Bayesian inference when the double exponential error structure, i.e., $\beta_i = 1$, was assumed. The data points from January 2003 to December 2004 were used in Bayesian conditioning; the rest of data, including the derived GPP from April 1994 to December 2006, were used for verification.

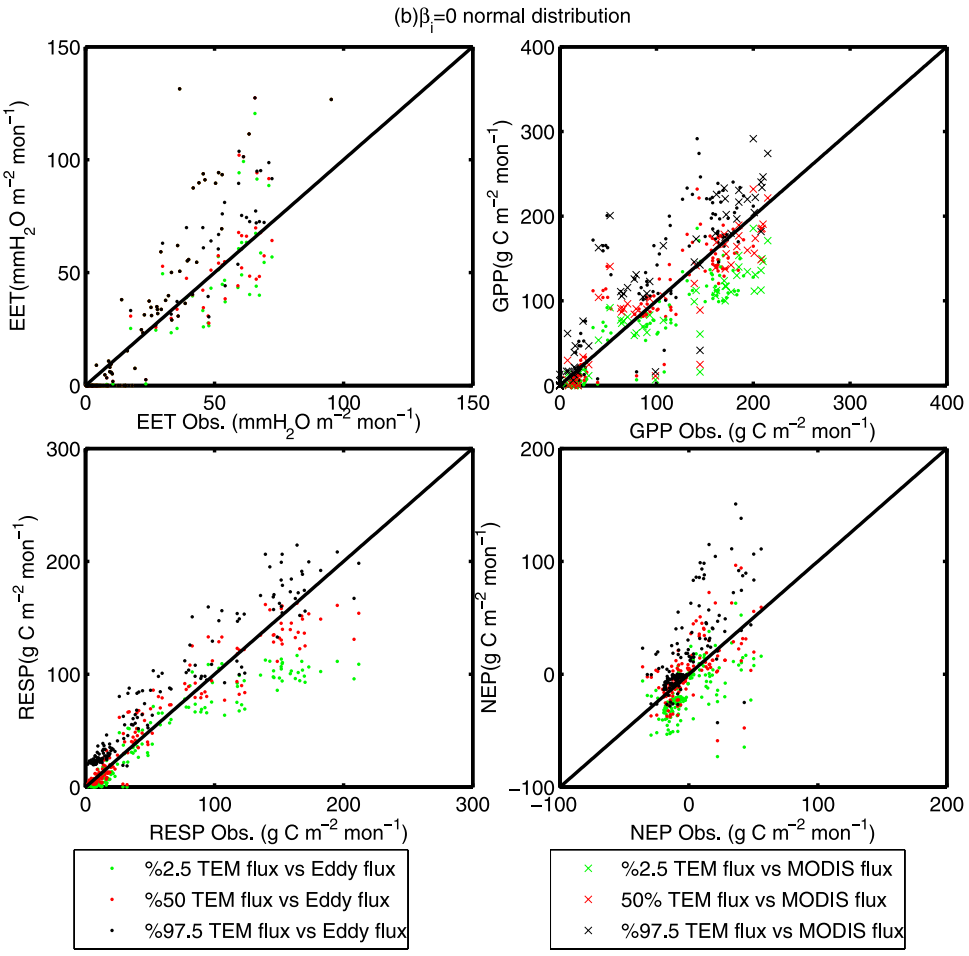

Figure 8b. Same as for Figure 8a, but the normal error structure, i.e., $\beta_i = 0$, was assumed.

binations of MODIS GPP flux data, the measured NEP, and the derived flux RESP. The effects of data error structures (measurement/derivation uncertainty) of C and EET fluxes on Bayesian inferences were examined using three different β_i values, which are 1 (double exponential distribution), 0 (normal distribution), and $-1/3$ (near-uniform distribution), for the likelihood function (equation (6)).

[32] We examined how the uncertainty of TEM parameters was reduced with the Bayesian inference technique by calculating the modes (the maximum posteriori) and the 95% credible intervals (or confidence intervals) of the posterior distributions, as well as the percentage change in the 95% credible intervals of the parameters. The percentage change in the 95% credible intervals was calculated as the difference between the 95% credible interval length of the prior and posterior distributions divided by the 95% credible interval length of the prior distribution. A positive percentage change in the 95% credible interval indicates the posterior has less uncertainty than the prior, and a negative change means the parameter is poorly constrained or edge-hitting. In addition, the percentage changes in the relative displacement of the parameters marginal distribution were also calculated according to the following formula

$$\delta_\theta = \sqrt{\int \left(\Pr(\theta) \log \frac{2\Pr(\theta)}{\Pr(\theta) + \Pr(\theta|V)} + \Pr(\theta|V) \log \frac{2\Pr(\theta|V)}{\Pr(\theta) + \Pr(\theta|V)} \right) d\theta} \quad (13)$$

as an assessment of the change from the shape of the parameter's prior marginal distribution $\Pr(\theta)$ to that of the posterior marginal distribution $\Pr(\theta|V)$ after Bayesian inference. The percentage change in displacement was normalized with the maximum of δ_θ, which is equal to $(2\log 2)^{1/2}$ [*Endres and Schindelin*, 2003]. Therefore a significant change in distribution shape after Bayesian inference would give a nonzero value, and a value of zero would correspond to no change in the distribution's shape.

[33] We examined how the uncertainty of model predictions of EET, GPP, RESP, and NEP was reduced by calculating the modes and 95% credible intervals for both simulations with the prior and the posterior parameters. The Root Mean Square Error (RMSE) and the coefficients of linear regression between the modes of the posterior TEM flux distributions, the TEM simulated fluxes with parameters obtained using the conventional calibration [e.g., *Raich et al.*, 1991], and the measured and derived data were also used to assess the improvement of the model predictability.

3. Results

3.1. Key Parameters to Influence Carbon Fluxes in TEM

[34] FOIR (first-order impact ratio) values indicate the importance of TEM parameters in affecting annual GPP, RESP, and NEP (Table 2). The CMAX, k_i, and k_c are the most important parameters (with FOIR > 5%) in determining

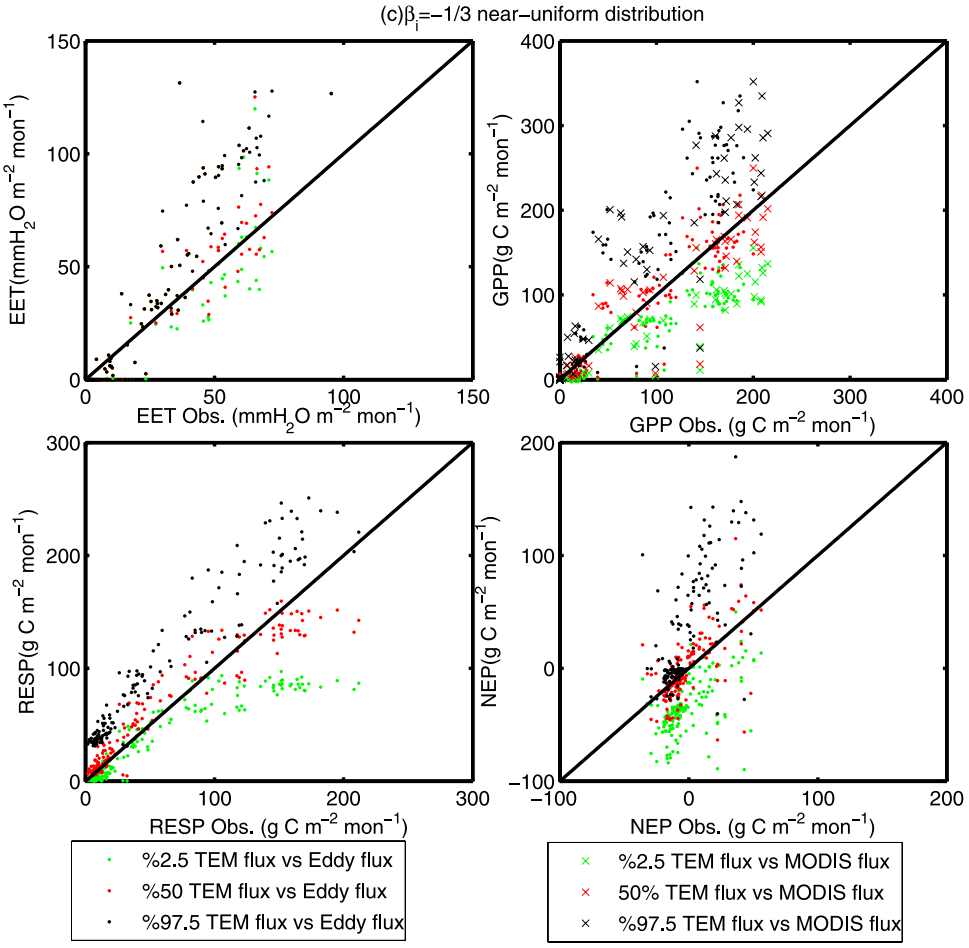

Figure 8c. Same as for Figure 8a, but the near-uniform error structure, i.e., $\beta_i = -1/3$, was assumed.

GPP. In contrast, the importance of CMAX, k_i, and k_c in determining RESP is mostly indirect, through their impact on R_A, the autotrophic respiration, which is related with GPP [*Raich et al.*, 1991]. During the growing season, for GPP and RESP, the FOIR of CMAX is greater than 0.3, suggesting the parameter explains more than 30% variation of these two fluxes (Figure 3). The impact of CMAX on NEP is complicated because of the interaction in GPP and RESP dynamics during the growing season. CMAX has the highest FOIR in June (>0.2) and the lowest in September (around 0.1), and its standard deviation deduced from the bootstrap analysis [*Davison and Hinkley*, 1997] is also highest for C flux simulations throughout the growing season. The parameter RHQ10, the exponential increase in R_H for every 10°C increase in temperature, also has high FOIR value, suggesting the importance of soil respiration R_H in determining NEP.

[35] The second group of important parameters (whose FOIR is less than 5% but greater than 0.5%) includes those related to phenology during the growing season (see Tables 1 and 2). Specifically, the CFALL and T_{min} are important to GPP, while CFALL, KRC and k_{n2} are important to RESP. For NEP, in addition to CFALL, KRC, k_{n2}, and T_{min}, parameter F_{ldcap} which controls the soil water availability in TEM, seems to be important. The FOIR values for parameters related to N dynamics (e.g., NMAX, NUP, k_{n1}, NFALL, except k_{n2}) are not high during the growing season (data not shown), implying that N cycling mostly manifests itself through the interaction with carbon cycling. This agrees with the algorithm in TEM that N cycling acts as a constraining or modulating process rather than a controlling process [*McGuire et al.*, 1997; *Tian et al.*, 1999]. In addition, the ranking of FOIRs suggests that the initial pool sizes of C and N in vegetation and soils are not important in constraining the uncertainty of simulated C fluxes (Table 2).

[36] For GPP, RESP and NEP, their sums of all FOIR values are less than 1.0 during the growing season (see Table 3). The FOIR sum for NEP is much smaller than those for GPP and RESP, leading us to analyze the interaction structure among parameters in the following section.

3.2. Interaction Structure of TEM Parameters

[37] The interaction structure of TEM parameters conditioned on EET observations and the MODIS GPP data indicates that there is a significant positive correlation between parameter k_c and CMAX (Figure 4a). This suggests a higher CO_2 uptake potential (denoted by CMAX) is associated with a higher half saturation point of CO_2 uptake (denoted by k_c). This agrees well with the quotient relationship between these two parameters [see *Raich et al.*, 1991, equation (1.6)] in the GPP formulation. However, the negative correlation between parameter k_c and k_i, as expected from the product relationship between the two,

Table 5. Root Mean Square Errors (RMSE), the Slope, Intercept, and R^2 Coefficient of the Linear Regression of the TEM Flux Modes Against Eddy Flux Tower Data and MODIS GPP When Different Types of Flux Data Are Used in Bayesian Inference Analyses[a]

	RMSE		Slope		Interception		R^2	
Inference Strategy	03-04	94-06	03-04	94-06	03-04	94-06	03-04	94-06
EET Flux Data								
NEP and EET	8.2	17.5	0.85	0.60	5.4	7.9	0.82	0.77
MODIS GPP, NEP, and EET	8.2	17.5	0.85	0.60	5.4	7.9	0.82	0.77
MODIS GPP, RESP, and EET	8.3	17.6	0.87	0.60	5.4	8.2	0.82	0.75
Base value simulation	16.8	24.4	0.51	0.51	6.4	6.6	0.86	0.89
GPP Flux Data								
NEP and EET	49.5	60.0	1.91	1.92	8.86	14.97	0.76	0.65
MODIS GPP, NEP, and EET	17.6	24.9	0.96	0.91	1.30	4.69	0.93	0.87
MODIS GPP, RESP, and EET	7.9	24.3	0.96	0.93	2.03	5.31	0.92	0.88
Base value simulation	21.7	27.0	0.89	0.86	−1.20	1.54	0.91	0.88
MODIS GPP Data								
NEP and EET	67.6	67.0	2.58	2.27	9.40	9.60	0.89	0.72
MODIS GPP, NEP, and EET	27.7	29.2	1.20	0.95	3.71	−0.63	0.93	0.86
MODIS GPP, RESP, and EET	28.4	25.9	1.20	1.04	4.65	2.13	0.93	0.89
Base value simulation	21.7	29.2	0.89	0.95	−1.20	−0.63	0.91	0.86
RESP Flux Data								
NEP and EET	50.9	63.7	4.68	5.29	−49.77	−57.47	0.72	0.68
MODIS GPP, NEP, and EET	13.0	16.7	0.98	1.00	1.05	1.54	0.93	0.92
MODIS GPP, RESP, and EET	12.2	17.9	1.06	1.09	0.76	1.08	0.95	0.92
Base value simulation	18.0	21.5	1.09	1.12	−10.19	−12.15	0.89	0.88
NEP Flux Data								
NEP and EET	5.3	13.4	0.90	0.70	1.03	−1.13	0.94	0.58
MODIS GPP, NEP, and EET	9.7	20.3	0.75	0.44	0.08	−1.18	0.83	0.32
MODIS GPP, RESP, and EET	9.9	20.2	0.74	0.46	−1.63	−2.46	0.85	0.40
Base value simulation	14.4	23.5	0.60	0.39	−0.16	−1.64	0.77	0.40

[a]Also given are the RMSE, the slope, intercept ,and R^2 coefficient of the linear regression of TEM simulated flux with parameters at their base values against MODIS GPP and eddy flux tower data. Data points from January 2003 to December 2004 are used in Bayesian inference. The linear regressions are conducted for the training period 03-04, and the overall period 94-06, respectively. All values are statistically significant ($p < 0.001$). Units for EET are mm H_2O m^{-2} mon^{-1}. Units for carbon fluxes are g C m^{-2} mon^{-1}.

is not revealed [*Raich et al.*, 1991]. Rather, a small positive correlation is found, contrary to the GPP formulation that for a fixed capability of C uptake, a lower half saturation point of photosynthetically active radiation (PAR) should be accompanied by a higher half saturation point of CO_2 uptake by plants. To test if a longer time series of GPP data can help show the expected negative interaction structure, we conducted a number of inference analyses with longer time series of GPP data and found the negative correlation between k_c and k_i were indeed well identified, but the overall interaction structure is different from that obtained when partition information is used (data not shown). The interactions between N related parameters and the ones related to C dynamics (data not shown) are difficult to interpret due to the complex structure of TEM and the lack of data for constraint. Not surprisingly, the N related parameters are either poorly constrained or edge-hitting (Table 4). When EET and NEP were used to deduce the interaction structure, much less correlation was obtained among the parameters (Figure 4b). Our further analyses indicated that a longer time series of these fluxes data does not help either to characterize the interaction structure of the parameters, though the positive correlation between k_c and CMAX still exists. This suggests that by only using one type of C flux data (i.e., NEP or MODIS GPP and EET) in Bayesian analysis, we cannot fully reveal the interaction structures between the parameters, such as, the quotient relationship between k_c and k_i, derived from empirical studies [*Raich et al.*, 1991]. Thus this explains that when only the observed EET and NEP were used in Bayesian inference (see Figure 9a), the NEP agrees well with measurements, but the simulated GPP and RESP are significantly different from the observed data. The same argument is also valid for the case that when EET and MODIS GPP were used in Bayesian inference, the RESP and NEP are very different from the observed data (result not shown). Conditioning TEM simulations on EET, NEP and MODIS GPP data (or other combinations of GPP and RESP partitioned from NEP) provides better interaction structures of parameters in comparison to other simulations (e.g., Figure 4). For example, the deduced large negative correlation (−0.5) between k_c and k_i suggests that proper combination of data that incorporates partition information of GPP and RESP from observed NEP should be used in Bayesian inference to well characterize the interaction structure of TEM parameters.

3.3. Reduced Uncertainty of Parameters

[38] With assumption of a normal error distribution (i.e. $\beta_i = 0$) for observed or derived flux data, the 95% credible intervals for all parameters were calculated with Bayesian inference framework using the two-year (2003–2004) data of EET, MODIS GPP and NEP (Table 4). The percentage changes of the 95% credible interval length for most parameters are small or moderate, suggesting the flux data are not able to well reduce the uncertainty of most parameters (Figure 5a). For instance, W_{iltpt} almost has the same amount of uncertainty from prior to posterior, whereas the

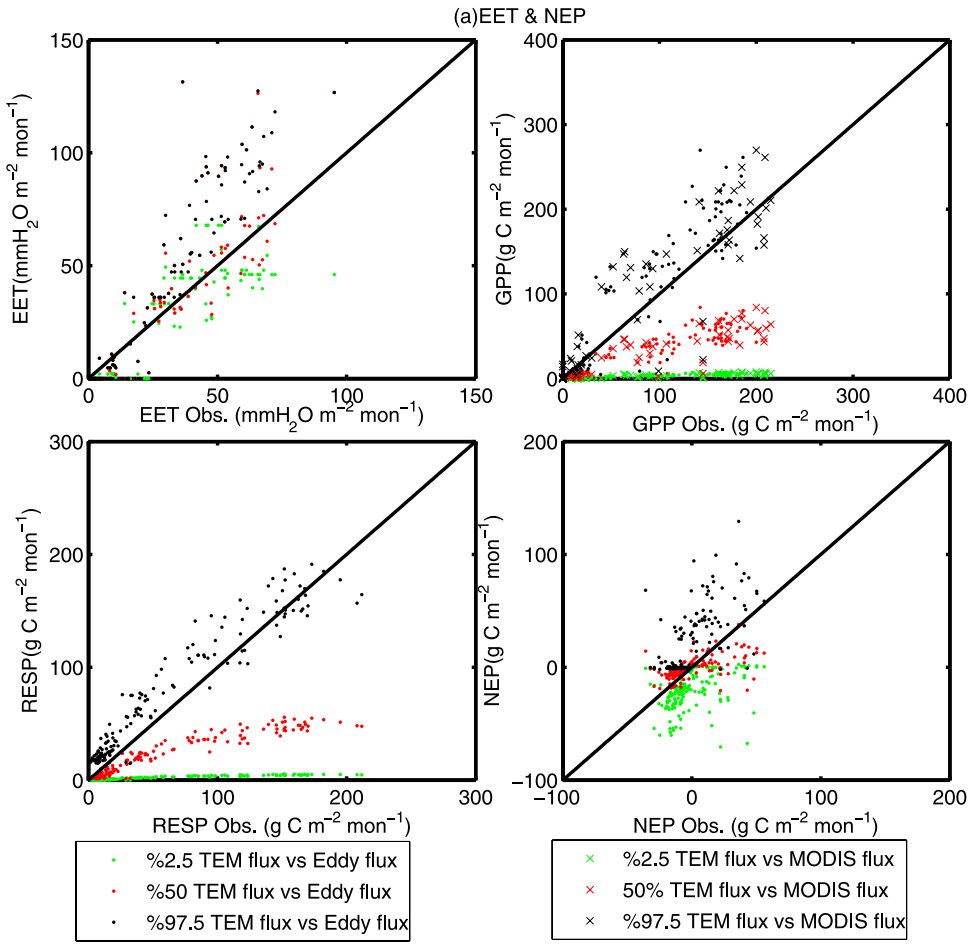

Figure 9a. Scatterplots of the posterior TEM outputs against observations after the Bayesian inference with the combination of EET and NEP data being used for conditioning. Data points from January 2003 to December 2004 were used in the Bayesian conditioning.

posterior of T_{max} even has negative percentage change (two-side edge-hitting) in its 95% credible interval when compared with its prior uniform distribution due to the parameter interactions. In contrast, nearly 30% or more changes occur for RAQ10A0, CMAX, T_{min}, KRC and R_{ootz}. CMAX, KRC and T_{min} have relatively high or moderate FOIR values during the growing season. The changes in the 95% credible intervals of RAQ10A0 and R_{ootz} are caused by their correlations with other parameters (see Figure 4c). This suggests that it is important to consider the parameter interactions in quantifying the uncertainty of model simulations.

[39] We obtained four values for each parameter after the implementation of Bayesian inference at statistical levels of 2.5%, 50% or median, and 97.5% as well as the mode (see Table 4). The modes represent the most likely values for parameters corresponding to the best fit between TEM simulations and the observed fluxes. Thus we may use this set of parameters as "true" parameters for TEM applications. This Bayesian inference-based parameterization method fully makes use of the available observed and derived flux data. If the new observed data are available, the parameters are readily updated and the uncertainty of parameters will be further reduced.

[40] The percentage change in the relative distance between the prior and posterior marginal distributions indicates that most parameters changed their shapes moderately and, some parameters changed their shapes negligibly, after the Bayesian inference (Figure 5b). This suggests that the observed data only exert limited constraints on TEM parameters using Bayesian inference.

[41] Using changes in 95% credible interval length and the shape of the marginal distribution, in conjunction with the normalized frequency plot (Figure 6), we were able to sort the posterior parameters into three classes, which are well-constrained (WC), poorly constrained (PC) and edge-hitting (EH) parameters (Table 4). The well-constrained parameters show a good convergence with a unimodal shape in their frequency plot. The poorly constrained parameters show either a flat shape or a multimodal shape. Most parameters are poorly constrained (small percent changes in shape or multimodal, see Figure 6b). Specifically, parameters R_{ootz}, T_{min}, RAQ10A0, RHQ10, CMAX and KDC are well-constrained (Figure 6a) and parameters C_v, k_i, T_{max}, RAQ10A3, CFALL and VEGC2N are edge-hitting (Figure 6c). Well-constrained parameters are closely related to algorithms of GPP formulae or autotrophic or heterotrophic respiration processes in TEM. Many parameters are moderate or poorly constrained, due to (1) they are

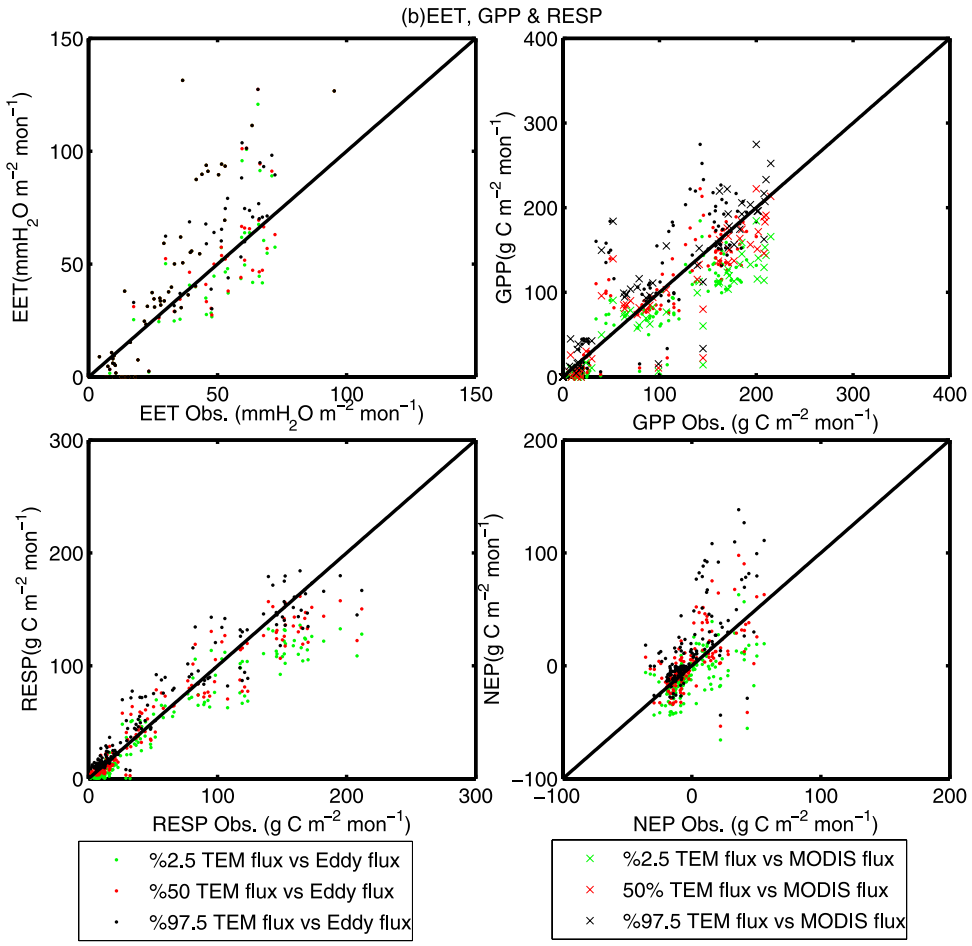

Figure 9b. Same as for Figure 9a, but the combination of EET, RESP, and MODIS GPP data used in Bayesian inference.

not directly related to algorithms of carbon uptake or release or (2) they often greatly interact with each other (e.g., with k_c), so that the flux data are not able to well constrain them.

[42] The base values of parameters developed through the conventional calibration are different from the statistical mode, i.e., the parameters which produce the best fit between TEM simulations and the observed flux data, and are mostly within the posterior 95% credible intervals (Figure 6 and Table 4).

3.4. Reduced Uncertainty of Model Predictions

[43] The median values at 50% statistical level and the bounds of 95% credible intervals of the posterior C fluxes, including GPP, RESP, and NEP indicate that the uncertainty range of the posterior is remarkably reduced in comparison to the simulations using the prior parameters (see Figure 2 and Figures 7 and 8a, 8b and 8c). The comparisons of C fluxes between modes of the Monte Carlo simulations and the eddy fluxes data indicate that TEM is able to more accurately reproduce the observed data depending on the type of the fluxes data used in the Bayesian inference framework (Table 5). Specifically, NEP is improved when both the MODIS GPP and the observed NEP and EET were used in our Bayesian inference analysis. When only the observed flux data NEP and EET were used in Bayesian inference, the mode NEP of the Monte Carlo simulations has the least RMSE, the linear regression coefficient is closest to 1.0, and the R-square value is highest. However, the posterior GPP and RESP are significantly different from the flux data in both the verification and Bayesian inference periods due to lack of constraint on the correlations among the parameters (Table 5 and Figures 9a–9b). For EET, the TEM simulations always appeared greater than the measurements, which may be due to underestimation of measurements of these fluxes [*Amthor et al.*, 2001], or due to the simple algorithms of EET in TEM [*Melillo et al.*, 1993].

4. Discussion

4.1. Effect of Data Error Structures on Parameter Estimation and Model Prediction

[44] One of the uncertainty sources for model predictions is the errors in the measured and derived data. Here we further examined how error structures of data affect parameter estimation and model prediction of TEM. We used three different values of β_i to represent different error structures associated with the eddy flux data in our Bayesian inference analysis. They are 1, 0, $-1/3$, which mathematically correspond to the double exponential distribution, normal distribution and near-uniform distribution. Not surprisingly, the three sets of analyses result in different uncertainty ranges and modes for the TEM posterior simulations of EET, GPP,

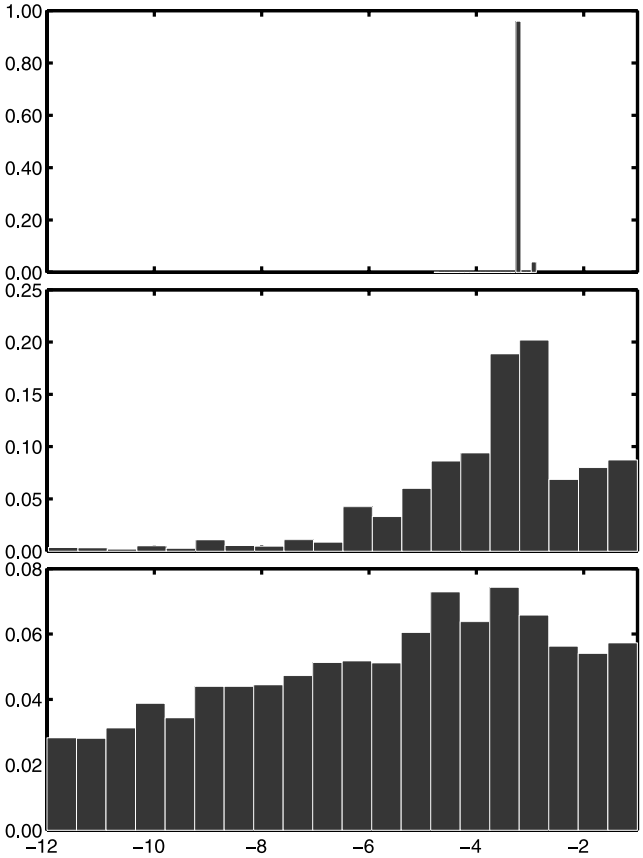

Figure 10. Normalized frequency plots for posterior T_{min} when different error structures were used to compute the likelihood functions.

RESP, and NEP (Table 5 and Figures 8a–8c). Specifically, among the three sets of analyses, the one with double exponential error distribution (i.e., $\beta_i = 1$) has the least uncertainty range and the one with near-uniform error distribution (i.e., $\beta_i = -1/3$) has the greatest uncertainty range, for the posterior of all the fluxes being analyzed; and the mode of the case with near-uniform error distribution fits the data worse than those from the cases with double exponential error distribution and normal error distribution. If more data points were used in the Bayesian inference, the simulated mode fluxes inferred with greater value of β_i are closer to the eddy flux data, and the posterior distributions of the parameters are skewed into narrower shapes (e.g., Figure 10). The one with normal error distribution (i.e. $\beta_i = 0$) has its mode close to the eddy flux data, except EET, and all the eddy flux data are inside the uncertainty range (see Figure 7 and Table 5) while its posterior parameters are not overconstrained (e.g., Figure 10); thus it is chosen as the best inference of this study. The impact of different error structures on the posterior parameters is similar to that on the posterior fluxes. For instance, the well-constrained parameter T_{min} is overconstrained when the double exponential error distribution is used in computing the likelihood function (see Figure 10). The posterior of T_{min} for the case with a near-uniform error distribution is too divergent because of the overestimation of data error. The normal error distribution resulted in parameters having a good convergence in posterior shapes, in addition to the good agreement of posterior fluxes with the eddy flux data. Overall, it suggests that the developed framework is capable of analyzing the effect of error structure of the eddy flux data on the uncertainty of parameters and model predictions. If the error structures of the observed data are available, we could use both observed mean values and their associated errors in our Bayesian analyses.

[45] *Williams et al.* [2005] pointed out that the correct estimation of observational errors was crucial to the quality of their results from the ensemble Kalman filter technique used in their model-data fusion analysis, because the magnitude of observational errors determines to what extent the simulated fields will be corrected to match the observations. The error variances are often specified by knowledge of instrumental characteristics or generated from replicate samples while the error correlations are often assumed to be zero. Similarly, *Raupach et al.* [2005] have stressed the importance of specifying the data uncertainty (errors) in model-data fusion analysis as the errors affect the eventually predicted uncertainty of the parameters and model outputs. They also pointed out the challenges in evaluating the uncertainty properties of observational data including error magnitudes, error correlations among observations, temporal structure of the observation errors and error distributions (e.g., Gaussian versus lognormal etc.). For example, in their implementation of Metropolis algorithms, *Braswell et al.* [2005] fixed an error for their data points due to the lack of necessary information to determine how errors vary in each data point. Our study provides an example of how to analyze the impact of different error structures on the posterior with our Bayesian inference framework, together with the parameterized likelihood function equation (6).

4.2. Data Selection for the Bayesian Inference

[46] An important contribution of this study is to provide a method for examining how different eddy fluxes affect the Bayesian inference analysis, thus improving model parameters and predictability. Here we conducted different sets of analyses conditioned on different combinations of the observed and derived flux data. When no partitioning information of eddy flux NEP is used, the posterior distributions of EET, GPP, RESP, and NEP, including their modes and bounds, are different from that when partitioning information is used (Figures 8a–8c and 9a–9b and Table 5). Among the three sets of combinations, the combination of EET and NEP is the least informative (Figure 4 and Table 5). When NEP was replaced with data containing NEP partitioning information (e.g., component RESP) and the MODIS GPP, the inference provides a similar mode to the one derived using NEP, MODIS GPP, and EET in inference analysis (Table 5), but the uncertainty bounds are slightly different due to the stochastic property of the Bayesian inference.

[47] The partitioned component RESP of the measured NEP could introduce useful information to constrain TEM, in conjunction with the MODIS GPP (Figures 4, 7, 8a–8c and 9a–9b). Our results showed that, in order to derive the reasonable inference of TEM parameters, the flux data used should at least have enough information to constrain parameters controlling the ecosystem production and respiration. This conclusion is also supported from another finding in

our experiment (results not shown) that if we use data of MODIS GPP in the growing season together with RESP in the nongrowing season in Bayesian analysis, the inference is still able to show the interaction structure among the parameters.

5. Conclusion

[48] We developed an integrated framework of global sensitivity analysis and Bayesian inference to analyze and improve parameterization and predictability of a monthly time step biogeochemistry model TEM. Using the framework, we were able to, for the first time, identify the key parameters of TEM model and examine the interaction structures of parameters and their effects on seasonal C dynamics. We showed that the improved parameterization of TEM could substantially reduce the uncertainty of C flux simulations in comparison with eddy flux data. We found that, unlike ecosystem models operated at a finer time step [e.g., *Santaren et al.*, 2007], the NEP measurement alone is able to constrain the estimated C fluxes, the partition information of GPP and RESP, or satellite-based GPP besides monthly NEP should also be used in Bayesian inference analysis to constrain coarse-time step ecosystem models such as TEM. Further, the assumed error structures of the flux data resulted in different uncertainty bounds of the posterior parameters and model predictions, suggesting that the error structure of the observed data should be developed and used in Bayesian inference analysis. We conclude that the developed Bayesian inference framework could be used to improve parameterization and predictability of relatively coarse time step biogeochemistry models when eddy flux data and other data (e.g., satellite-based) and their associated errors are available.

[49] **Acknowledgments.** The research is supported by the National Science Foundation with projects of NSF-0554811 and NSF-0630319 to Q.Z. and the Graduate Fellowship from the Purdue Climate Change Research Center and the Graduate Fellowship from the NASA Earth System Science Fellowship program to J.T. The high-performance computing for this research is provided by the Rosen Center for Advanced Computing at Purdue University. We thank Ian Enting and another three anonymous reviewers for their invaluable comments on the earlier versions of the manuscript. We also thank Dr. Wofsy's group at Harvard University for providing the CO_2 flux data for this study. The authors express their gratitude to Rose Filley for helping in the language editing to improve the manuscript.

References

Aalto, T., P. Ciais, A. Chevillard, and C. Moulin (2004), Optimal determination of the parameters controlling biospheric CO_2 fluxes over Europe using eddy covariance fluxes and satellite NDVI measurements, *Tellus*, *56B*, 93–104.

Amthor, J. S., et al. (2001), Boreal forest CO_2 exchange and evapotranspiration predicted by nine ecosystem process models: Intermodel comparisons and relationships to field measurements, *J. Geophys. Res.*, *106*(D24), 33,623–33,648.

Balshi, M. S., et al. (2007), The role of historical fire disturbance in the carbon dynamics of the pan-boreal region: A process-based analysis, *J. Geophys. Res.*, *112*, G02029, doi:10.1029/2006JG000380.

Bates, S. C., A. E. Raftery, and A. C. Cullen (2000), Bayesian uncertainty assessment in deterministic models for environmental risk assessment, *NRCSE Tech. Rep. Ser.*, *58*, 17 pp., U.S. Environ. Prot. Agency, Washington, D. C.

Beven, K., and J. Freer (2001), Equifinality, data assimilation, and uncertainty estimation in mechanistic modeling of complex environmental systems using the GLUE methodology, *J. Hydrol.*, *249*, 11–29.

Box, G. E. P., and G. C. Tiao (1973), *Bayesian Inference in Statistical Analysis*, Addison-Wesley, Reading, Mass.

Braswell, B. H., W. J. Sacks, E. Linder, and D. S. Schimel (2005), Estimating diurnal to annual ecosystem parameters by synthesis of a carbon flux model with eddy covariance net ecosystem exchange observations, *Global Change Biol.*, *11*, 335–355.

Clein, J. S., A. D. McGuire, X. Zhang, D. W. Kicklighter, J. M. Mellio, S. C. Wofsy, P. G. Javis, and J. M. Massheder (2002), Historical and projected carbon balance of mature black spruce ecosystems across North America: The role of carbon-nitrogen interactions, *Plant and Soil*, *242*, 15–32.

Davison, A. C., and D. V. Hinkley (1997), *Bootstrap Methods and Their Application*, Cambridge Univ. Press, Cambridge, New York.

Dunn, A. L., C. C. Barford, S. C. Wofsy, M. L. Goulden, and B. C. Daube (2007), A long-term record of carbon exchange in a boreal black spruce forest: Means, responses to interannual variability, and decadal trends, *Global Change Biol.*, *13*, 577–590.

Endres, D. M., and J. E. Schindelin (2003), A new metric for probability distribution, *IEEE Trans. Inf. Theory*, *49*(7), 1858–1860.

Euskirchen, E. S., et al. (2006), Importance of recent shifts in soil thermal dynamics on growing season length, productivity, and carbon sequestration in terrestrial high-latitude ecosystems, *Global Change Biol.*, *12*, 731–750.

Frolking, S., et al. (1996), Modeling temporal variability in the carbon balance of a spruce/moss boreal forest, *Global Change Biol.*, *2*, 343–366.

Gordon, N. J., D. J. Salmond, and A. F. M. Smith (1993), Novel approach to nonlinear/non-Gaussian Bayesian state estimation, *IEE Proc. F*, *140*, 107–113.

Goulden, M. L., B. C. Daube, S. M. Fan, D. J. Sutton, A. Bazzaz, J. W. Munger, and S. C. Wofsy (1997), Physiological response of a black spruce forest to weather, *J. Geophys. Res.*, *102*(D24), 28,987–28,996.

Goulden, M. L., et al. (1998), Sensitivity of boreal forest carbon balance to soil thaw, *Science*, *279*, 214–217.

Green, E. J., D. W. MacFarlane, H. T. Valentine, and W. E. Strawderman (1999), Assessing uncertainty in a stand growth model by Bayesian synthesis, *For. Sci.*, *45*, 528–538.

Hong, B., R. L. Strawderman, D. P. Swaney, and D. A. Weinstein (2005), Bayesian estimation of input parameters of a nitrogen cycle model applied to a forested reference watershed, Hubbard Brook Watershed Six, *Water Resour. Res.*, *41*, W03007, doi:10.1029/2004WR003551.

Iman, R. L., and W. J. Conover (1982), A distribution-free approach to inducing rank correlation among input variables, *Commun. Stat.: Part B. Simulation Comput.*, *11*, 311–334.

Iman, R. L., and J. C. Helton (1988), An investigation of uncertainty and sensitivity analysis techniques for computer models, *Risk Anal.*, *8*, 71–90.

Kaheil, Y. H., M. K. Gill, M. McKee, and L. Bastidas (2006), A new Bayesian recursive technique for parameter estimation, *Water Resour. Res.*, *42*, W08423, doi:10.1029/2005WR004529.

Knorr, W., and J. Kattge (2005), Inversion of terrestrial ecosystem model parameter values against eddy covariance measurements by Monte Carlo sampling, *Global Change Biol.*, *11*, 1333–1351.

Kuczera, G., and E. Parent (1998), Monte Carlo assessment of parameter uncertainty in conceptual catchment models: The Metropolis algorithm, *J. Hydrol.*, *221*, 69–95.

McGuire, A. D., J. M. Melillo, L. A. Joyce, D. W. Kicklighter, A. L. Grace, B. Moore III, and C. J. Vorosmarty (1992), Interactions between carbon and nitrogen dynamics in estimating net primary productivity for potential vegetation in North America, *Global Biogeochem. Cycles*, *6*(2), 101–124.

McGuire, A. D., J. M. Melillo, D. W. Kicklighter, Y. Pan, X. Xiao, J. Helfrich, B. Moore III, C. J. Vorosmarty, and A. L. Schloss (1997), Equilibrium responses of global net primary production and carbon storage to doubled atmospheric carbon dioxide: Sensitivity to changes in vegetation nitrogen concentration, *Global Biogeochem. Cycles*, *11*(2), 173–189.

McGuire, A. D., et al. (2001), Carbon balance of the terrestrial biosphere in the twentieth century: Analyses of CO_2, climate and land-use effects with four process-based ecosystem models, *Global Biogeochem. Cycles*, *15*(1), 183–206.

Melillo, J. M., A. D. McGuire, D. W. Kicklighter, B. Moore III, C. J. Vorosmarty, and A. L. Schloss (1993), Global climate change and terrestrial net primary production, *Nature*, *63*, 234–240.

O'Neill, K. P., E. S. Kasischke, and D. D. Richter (2003), Seasonal and decadal patterns of soil carbon uptake and emission along an age sequence of burned black spruce stands in interior Alaska, *J. Geophys. Res.*, *108*(D1), 8155, doi:10.1029/2001JD000443.

Poole, D. J., and A. E. Raftery (2000), Inference for deterministic simulation models: The Bayesian melding approach, *J. Am. Stat. Assoc.*, *95*, 1244–1255.

Potter, C. S., R. J. Randerson, C. B. Field, P. A. Matson, P. M. Vitousek, H. A. Mooney, and S. A. Klooster (1993), Terrestrial ecosystem production: A process model based on global satellite and surface data, *Global Biogeochem. Cycles*, *7*(4), 811–842.

Raich, J. W., E. B. Rastetter, J. M. Melillo, D. W. Kicklighter, P. A. Steudler, B. J. Peterson, A. L. Grace, B. Moore III, and C. J. Vorosmarty (1991), Potential net primary productivity in South America: Application of a global model, *Ecol. Appl.*, *1*, 399–429.

Ratto, M., S. Tarantola, and A. Saltelli (2001), Sensitivity analysis in model calibration: GSA-GLUE approach, *Com. Phys. Comm.*, *136*, 212–224.

Raupach, M. R., P. J. Rayner, D. J. Barrett, R. S. DeFries, M. Heimann, D. S. Ojima, S. Quegan, and C. C. Schmullius (2005), Model-data synthesis in terrestrial carbon observation: Methods, data requirements and data uncertainty specifications, *Global Change Biol.*, *11*, 378–397.

Running, S. W., and J. C. Coughlan (1988), General model of forest ecosystem processes for regional applications: I. Hydrologic balance, canopy gas exchange and primary production processes, *Ecol. Modell. ECMOOT*, *42*, 125–154.

Running, S. W., and E. R. J. Hunt (1993), Generalization of a forest ecosystem process model for other biomes, BIOME-BGC and an application for global-scale models, in *Scaling Physiological Processes: Leaf to Globe*, edited by J. R. Ehleringer and C. B. Field, pp. 141–158, Academic, San Diego, Calif.

Running, S. W., R. R. Nemani, F. A. Heinsch, M. Zhao, M. Reeves, and H. Hashimoto (2004), A continuous satellite-derived measure of global terrestrial production, *BioScience*, *54*, 547–560.

Saltelli, A., S. Tarantola, F. Campolongo, and R. Marco (2004), *Sensitivity Analysis in Practice: A Guide to Assessing Scientific Models*, Wiley, Chichester, U. K.

Santaren, D., P. Peylin, N. Viovy, and P. Ciais (2007), Optimizing a process-based ecosystem model with eddy-covariance flux measurements: A pine forest in southern France, *Global Biogeochem. Cycles*, *21*, GB2013, doi:10.1029/2006GB002834.

Sellers, P. J., et al. (1997), BOREAS in 1997: Experiment overview, scientific results, and future directions, *J. Geophys. Res.*, *102*(D24), 28,731–28,769.

Skare, Ø., E. Bølviken, and L. Holden (2003), Improved sampling-importance resampling and reduced bias importance sampling, *Scand. J. Stat.*, *30*, 719–737.

Thiemann, M., M. Trosser, H. Gupta, and S. Sorooshian (2001), Bayesian recursive parameter estimation for hydrologic models, *Water Resour. Res.*, *37*(10), 2521–2536.

Tian, H., J. M. Melillo, D. W. Kicklighter, A. D. McGuire, and J. Helfrich (1999), The sensitivity of terrestrial carbon storage to historical climate variability and atmospheric CO_2 in the United States, *Tellus*, *51B*, 414–452.

Turner, D. P., et al. (2006), Evaluation of MODIS NPP and GPP products across multiple biomes, *Remote Sens. Environ.*, *102*, 282–292.

Van Cleve, K. L., C. T. Dyrness, L. A. Viereck, J. Fox, F. S. Chapin III, and W. Oechel (1983), Taiga ecosystems in interior Alaska, *BioScience*, *33*, 39–44.

VEMAP Members (1995), Vegetation/Ecosystem Modeling and Analysis Project: Comparing biogeography and biogeochemistry models in a continental-scale study of terrestrial ecosystem responses to climate change and CO_2 doubling, *Global Biogeochem. Cycles*, *9*(4), 407–437.

Wang, Y. P., R. Leuning, H. A. Cleugh, and P. A. Coppin (2001), Parameter estimation in surface exchange models using nonlinear inversion: How many parameters can be estimate and which measurements are most useful, *Global Change Biol.*, *7*, 495–510.

Wang, Y. P., D. Baldocchi, R. Leuning, E. Falge, and T. Vesala (2007), Estimating parameters in a land-surface model by applying nonlinear inversion to eddy covariance flux measurements from eight FLUXNET sites, *Global Change Biol.*, *13*, 652–670.

Weber, M. G., and K. van Cleve (1984), Nitrogen transformation in feather moss and forest floor layers of interior Alaska black spruce ecosystems, *Can. J. For. Res.*, *14*, 278–290.

Williams, M., P. A. Schwarz, B. E. Law, J. Irivne, and M. R. Kurpius (2005), An improved analysis of forest carbon dynamics using data assimilation, *Global Change Biol.*, *11*, 89–105.

Wofsy, S. C., and A. Dunn (2001), BOREAS Follow-On FLX-01 NSA-OBS Derived Data- NEP, GEP and Respiration, dataset available on-line at http://www.as.harvard.edu/chemistry/boreas/index.html, Oak Ridge Natl. Lab., Oak Ridge, Tenn.

Zhuang, Q., V. E. Romanovsky, and A. D. McGuire (2001), Incorporation of a permafrost model into a large-scale ecosystem model: Evaluation of temporal and spatial scaling issues in simulating soil thermal dynamics, *J. Geophys. Res.*, *106*(D24), 33,649–33,670.

Zhuang, Q., A. D. McGuire, K. P. O'Neill, J. W. Harden, V. E. Romanovsky, and J. Yarie (2002), Modeling the soil thermal and carbon dynamics of a fire chronosequence in interior Alaska, *J. Geophys. Res.*, *107*, 8147, doi:10.1029/2001JD001244, [printed *108*(D1), 2003].

Zhuang, Q., et al. (2003), Carbon cycling in extratropical terrestrial ecosystems of the Northern Hemisphere during the 20th century: A modeling analysis of the influences of soil thermal dynamics, *Tellus*, *55B*, 751–776.

Zhuang, Q., J. M. Melillo, D. W. Kicklighter, R. G. Prinn, A. D. McGuire, P. A. Steudler, B. S. Felzer, and S. Hu (2004), Methane fluxes between terrestrial ecosystems and the atmosphere at northern high latitudes during the past century: A retrospective analysis with a process-based biogeochemistry model, *Global Biogeochem. Cycles*, *18*, GB3010, doi:10.1029/2004GB002239.

Zhuang, Q., J. M. Melillo, M. C. Sarofim, D. W. Kicklighter, A. D. McGuire, B. S. Felzer, A. Sokolov, R. G. Prinn, P. A. Steudler, and S. Hu (2006), CO_2 and CH_4 exchanges between land ecosystems and the atmosphere in northern high latitudes over the 21st century, *Geophys. Res. Lett.*, *33*, L17403, doi:10.1029/2006GL026972.

J. Tang and Q. Zhuang, Purdue Climate Change Research Center, Purdue University, Civil Engineering Building, 550 Stadium Mall Drive, West Lafayette, IN 47907-2051, USA. (tang16@purdue.edu)